INTERNATIONAL ATOMIC ENERGY AGENCY
UNITED NATIONS EDUCATIONAL, SCIENTIFIC AND CULTURAL ORGANIZATION

INTERNATIONAL CENTRE FOR THEORETICAL PHYSICS
34100 TRIESTE (ITALY) - P.O.B. 586 - MIRAMARE - STRADA COSTIERA 11 - TELEPHONES: 224281/2/3/4/5/6
CABLE: CENTRATOM - TELEX 46392 ICTP

SMR-30/ 14

WINTER COLLEGE ON ATOMIC AND MOLECULAR PHYSICS

26 January - 18 March 1977

METHODS OF GENERATING PICOSECOND LIGHT PULSES

D.J. BRADLEY
Applied Optics Section
Imperial College
London, England

Uncorrected Page Proofs.

2. Methods of Generating Picosecond Light Pulses

D. J. Bradley

With 46 Figures

It is over a decade since picosecond laser pulses were first produced by passive modelocking of a giant-pulse ruby laser by *Mocker* and *Collins* [2.1] in 1965 and then Nd:glass lasers by *de Maria* et al. [2.2] in 1966. Since then the techniques for the generation of these pulses have been developed to the extent that it is possible to reliably produce pulses of bandwidth-limited durations of ~1 ps from both pulsed and cw lasers. In addition, theoretical models have been refined to the stage that there is excellent agreement with even the details of the experimental results, and there is now a very good understanding of the mechanisms by which ultrashort pulses evolve from the initial fluorescence intensity fluctuation patterns. These substantial advances in technology and physical understanding have been largely due to the simultaneous development of the methods of picosecond chronoscopy, particularly the direct linear measurement of pulse durations by electron-optical streak cameras. This pattern, of course, follows the historical pattern whereby developments in science and technology are almost always related to advances in measurement techniques. As a result the methods of picosecond laser pulse generation and measurement are now sufficiently refined and catalogued for them to be used with confidence for the investigation on a picosecond timescale of the interaction of coherent light with matter.

The purpose of this chapter is to summarize the present state of the art in picosecond pulse generation, dealing only with systems which are capable of producing pulses of durations ~10 ps or less. As a consequence, the methods of active modelocking of pulsed and continuous lasers are not considered, since such systems have to date not produced such short pulses. (Actively modelocked lasers have been extensively reviewed, [2.3, 4]). Also excluded are gas lasers, although pulses of durations ~100 ps have been obtained by actively modelocking the argon-ion laser [2.5] and the iodine photodissociation laser [2.6], and, from a passively modelocked high-pressure CO_2 laser [2.7], and it is likely that the newly developed broadband excimer and exciplex lasers based upon high-pressure gases (see Proceedings of Conference on High Power Gas Lasers 1975 [2.8]), will provide sources of picosecond pulses tunable throughout the uv.

The mathematical description of optical pulses is immediately followed by an account of the experimental methods of measuring temporal intensity profiles. Emphasis is placed upon the recently perfected electron-optical picosecond streak-camera techniques since these provide direct linear measure-

ments of pulses over a wide range of photon energies from ~ 1 eV to several keV. The two main types of picosecond sources, giant-pulse solid state systems and dye lasers, are then discussed together with the extensive and detailed experimental studies of the temporal buildup of modelocking of these lasers, including measurements of the properties of saturable absorbers and the effects of the nonlinear index of refraction. Special attention is paid to the cw dye laser, since this is the only source, to date, of steady-state, bandwidth-limited subpicosecond pulses. Recent developments of dye lasers, synchronously pumped by modelocked gas and solid-state lasers, are also described. The fluctuation model of passive-modelocking is related to these experimental studies, in particular to the special properties of dye lasers. Methods of picosecond pulse amplification and the limitations set by the linear and nonlinear properties of the laser media are described. Finally some of the latest results obtained in frequency changing picosecond pulses into the uv, vuv, and ir spectral regions by harmonic-generation and by nonlinear optical mixing are briefly considered theoretically and experimentally.

2.1 Optical Pulse Properties and Methods of Measurement

Before discussing the details of the generation of picosecond pulses, it is necessary to establish an appropriate mathematical description of the optical pulses themselves and to define the terminology involved. It is also sensible to follow this with a discussion of the methods available for the measurement of the temporal profile, the essential property of an ultrashort pulse.

2.1.1 General Description of Modelocked Laser Pulses

Perfect modelocking represents one of the two completely organised states of operation of a laser. To each transverse mode of a laser cavity there corresponds a set of longitudinal modes (Fig. 2.1), each having the same form of spatial energy distribution in a transverse plane, but with different distributions along the axis of the resonator. These longitudinal modes are separated in frequency by $c/2L$, where L is the optical pathlength between the mirrors and c is the velocity of light [2.9]. By employing appropriately designed laser resonators, including the use of apertures, single transverse-mode operation can be readily obtained. The addition of intracavity frequency-selective components [2.10] can then ensure operation of the laser in a single longitudinal, single transverse mode. The second completely organised situation occurs when the set of longitudinal modes is maintained in fixed phase and fixed amplitude relationships. In this case, the output will be a well-defined function of time, the modelocked laser pulse train. With a lasing medium of adequate bandwidth a regularly spaced train of picosecond pulses can be produced in this manner.

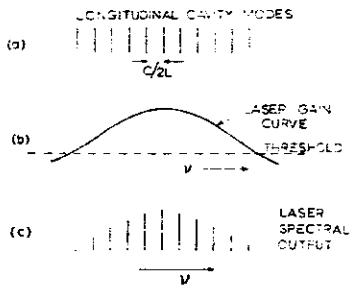

Fig. 2.1. Interaction of laser gain curve and longitudinal cavity modes resulting in oscillation at several resonator mode frequencies for which the laser gain is above the threshold value

Starting from the pair of Fourier integrals

$$E(t)=\frac{1}{\sqrt{2\pi}}\int_{-\infty}^{+\infty} e(\omega)\exp(-i\omega t)\,d\omega \tag{2.1}$$

and

$$e(\omega)=\frac{1}{\sqrt{2\pi}}\int_{-\infty}^{+\infty} E(t)\exp(i\omega t)\,dt \tag{2.2}$$

we define the complex signal $V(t)$ of a plane-wave optical pulse associated with the magnitude $E(t)$ of the electric field vector at a fixed point in space by writing [2.11, 12]

$$\begin{aligned} V(t)&=\frac{1}{\sqrt{2\pi}}\int_{0}^{\infty} 2e(\omega)\exp(-i\omega t)\,d\omega \\ &=\frac{1}{\sqrt{2\pi}}\int_{-\infty}^{+\infty} v(\omega)\exp(-i\omega t)\,d\omega. \end{aligned} \tag{2.3}$$

In obtaining (2.3) the amplitudes of the negative frequency components in the integral of (2.1) are suppressed and the amplitudes of the positive frequencies are doubled. It follows that

$$\begin{aligned} v(\omega)&=\frac{1}{\sqrt{2\pi}}\int_{-\infty}^{+\infty} V(t)\exp(+i\omega t)\,dt \\ &=2e(\omega)\quad(\omega>0) \\ &=0\qquad(\omega<0). \end{aligned} \tag{2.4}$$

The complex functions $V(t)$ and $v(\omega)$ can be employed to define an optical pulse in the time and frequency domains, respectively. By writing

$$v(\omega)=a(\omega)\exp\left[-i\phi(\omega)\right] \tag{2.5}$$

we define $a(\omega)$ the spectral amplitude and $\phi(\omega)$ the spectral phase [2.13]. When the pulse bandwidth $\Delta\omega$ is narrow compared with the mean optical frequency ω_0 we can write

$$V(t)=A(t)\exp i[\Phi(t)-\omega_0 t]. \tag{2.6}$$

In this quasi-monochromatic case, the temporal amplitude $A(t)$ and the temporal phase $\Phi(t)$ of the optical-frequency wave are both slowly varying functions of time. The instantaneous intensity is then

$$I(t)=V(t)V^*(t)=A^2(t). \tag{2.7}$$

By analogy, the spectral intensity function (recorded by a spectroscope or spectral analyser) can be defined as

$$i(\omega)=v(\omega)v^*(\omega)=a^2(\omega) \tag{2.8}$$

Since, by Parseval's theorem,

$$\int_{-\infty}^{+\infty} V(t)\exp(+i\omega t)\,dt \quad \int_{-\infty}^{+\infty} I(t)\,dt = \int_{0}^{\infty} a^2(\omega)\,d\omega, \tag{2.9}$$

the total energy of a pulse is proportional to the area under either of the, temporal or spectral, intensity profiles.

This notation clearly shows the symmetry between the temporal and frequency descriptions of an optical pulse. In each case, the structure of the pulse is completely defined by a phase and an intensity, and there is a one-to-one correspondence between the two intensity profiles, $I(t)$ and $i(\omega)$. The general relationship between the two functions arising from the Uncertainty Principle, is

$$(\Delta\omega\Delta t)/2\pi \geqslant K \tag{2.10}$$

where K is a constant of the order of unity, whose value depends upon the shapes of the intensity profiles. The shortest pulse obtainable with a given spectral bandwidth is described as being "transform-limited" or "bandwidth-limited". In this case the duration is

$$\Delta t=2\pi K(\Delta\omega)^{-1}. \tag{2.11}$$

The value of $(\Delta\omega\Delta t/2\pi)$, called the "time-bandwidth product" P, is a most important parameter in the study of ultrashort laser pulses, and is used as a measure of the extent to which the ideal modelocked situation has been achieved with a particular system. A "bandwidth-limited" pulse can also be defined physically as a pulse completely devoid of amplitude or frequency modulation.

A better understanding of the degree of organisation produced by modelocking may be obtained by considering the pictorial representation of the time and frequency descriptions given in Fig. 2.2 for the two cases of a non-modelocked laser and a perfectly modelocked laser, respectively. In generating these diagrams it was assumed [2.13] that the laser was operating with 101 discrete longitudinal modes, of equal frequency separation $\delta\omega$. In the time domain, the field pattern then repeats itself with a periodicity of $2\pi(\delta\omega)^{-1}$, corresponding to the double transit-time of the laser resonator, [2.14], even when the longitudinal modes are largely uncorrelated. In this quasi-periodical intensity fluctuation pattern, the duration of the shortest fluctuation is of the order of the inverse bandwidth. Below the lasing threshold, the amplitudes and phases of the cavity modes fluctuate randomly as a result of the independence of the different spontaneously emitting sources. While these fluctuations become progressively less marked as the threshold is passed and stimulated emission begins to dominate, each mode still remains largely uncorrelated with its neighbours and the temporal pattern is still very similar to that of thermal noise. In obtaining the computer simulation of Fig. 2.2a the 101 spectral phases were chosen randomly in the range $-\pi$ to $+\pi$ and the spectral intensities were generated with a Rayleigh distribution about a gaussian mean.

To achieve modelocked operation of the laser it is necessary to introduce some device that will correlate the spectral amplitudes and phases. Then the perfectly modelocked situation, also shown in Fig. 2.2, is obtained. For simplicity the spectral intensity was chosen to have a gaussian distribution

$$i(\omega)=\exp\left[-(\omega-\omega_0)^2/\alpha\right], \tag{2.12}$$

and the corresponding temporal intensity profile is then also gaussian

$$I(t)=\alpha\exp\left[-\alpha(t-t_0)^2\right]. \tag{2.13}$$

For this combination of intensity profiles $K=(2\ln 2)/\pi=0.441$ in (2.10) and (2.11). With care this ideal situation, resulting in a train of isolated, transform-limited pulses, can be achieved in practice with pulses as short as 0.3 ps (see *Modelocked cw Dye Lasers*).

While techniques and procedures for achieving good modelocking have evolved empirically over the years, it was only with the development of the picosecond electron-optical streak camera [2.13], with the capability of recording $I(t)$ directly with adequate time resolution, that a detailed understanding of the processes involved was obtained. The absence of this direct

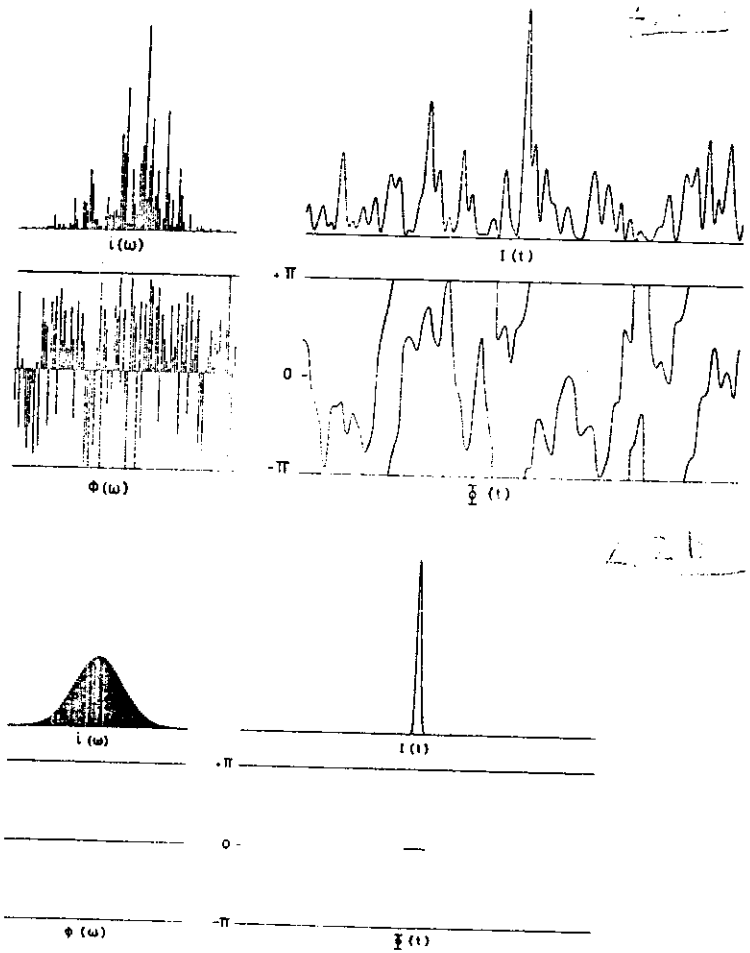

Fig. 2.2a and b. Simulation of the signal structure of (a) A non-modelocked laser, and (b) An ideally modelocked laser. In the frequency domain (left) in (a) the intensities $i(\omega)$ of the 101 discrete longitudinal modes have a Rayleigh distribution about a gaussian mean and the phases $\phi(\omega)$ are randomly distributed in the range $-\pi$ to $+\pi$. In the time domain (right) the phase $\bar{\phi}(t)$ fluctuates randomly, while the intensity $I(t)$ has the characteristics of thermal noise. In (b) the 101 spectral intensities have a gaussian distribution while the spectral phases are identically zero. In the time domain the signal is a bandwidth-limited gaussian pulse and the temporal intensity should be scaled up by $\underline{\times}20$ to correspond quantitatively with (a) (from *Bradley* and *New* [2.13])

measurement capability had resulted in erroneous reports of the generation of isolated picosecond and subpicosecond pulses by early experimenters, because they did not fully understand the precautions to be taken in applying the nonlinear correlation techniques then employed for pulse duration measurements. Because measurement of the temporal intensity profile $I(t)$ with picosecond time resolution has been the key to the understanding and development of modelocking techniques over the last decade, the state of the art of picosecond chronoscopy will be summarized before proceeding to a discussion of laser experiments.

2.1.2 Measurement of Pulse Intensity Profile I(t)

The simplest and most direct method of recording the temporal intensity profile of a light pulse is provided by the photodiode-oscilloscope combination. While the response time of the photoelectric effect is thought to be $\sim 10^{-14}$ s [2.15] the fastest real-time oscilloscopes have bandwidths of ~ 5 GHz, corresponding to a risetime of ~ 70 ps. Photodiodes with risetimes of ~ 100 ps and with current characteristics capable of driving such an oscilloscope are commercially available. As an example, a 10 GHz IMPATT silicon photodiode mounted in a coaxial cable has been employed to drive a 5 GHz oscilloscope with a sensitivity of 3 V cm^{-1} [2.16]. If the pulses to be measured are repetitive, as in cw modelocked lasers, and if real-time measurement of a single pulse is not required, pulse sampling techniques can be employed. In this case, the photodiode risetime limits the time resolution to 100 ps, since the oscilloscope sampling unit can have a risetime as short as 25 ps. Thus direct pulse measurements down to a time resolution of ~ 100 ps can be readily achieved. However, for experiments with modelocked lasers this performance is inadequate, and subpicosecond time resolution is required to diagnose presently available laser systems. This time resolution can only be achieved by nonlinear correlation methods or by electron-optical chronoscopy.

Two-Photon Fluorescence (TPF) Measurements

The nonlinear techniques for measuring the intensities of ultrashort pulses based upon the recording of the various correlation functions of $I(t)$ have been reviewed extensively. [2.13]. While the rapid development of ultrafast streak cameras has provided means for the direct recording of $I(t)$ with subpicosecond time resolution, nonlinear measurements are still widely employed, and most of the significant early results were obtained through their use. Since time measurements employing second-harmonic generation, especially of cw lasers, and the use of the optical Kerr-effect shutter are described in later chapters, it will be necessary to consider here only the two-photon fluorescence technique.

The widely employed two-photon fluorescence method [2.17] of ultrashort pulse duration measurement uses the experimental arrangement shown in

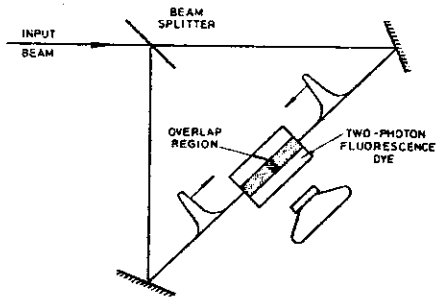

Fig. 2.3. The triangular configuration for the two-photon fluorescence (TPF) method of picosecond pulse duration measurement. The alignment of the optical triangle is critical if good results are to be obtained

Fig. 2.3. Each pulse of a train, or a single switched-out pulse, is split into two pulses of equal intensity which, in the usual triangular arrangement, overlap in a dye cell. The dye is chosen so that it can be excited to fluorescence by light of the laser wavelength only by two-photon absorption. The intensity of the fluorescence subsequently emitted is then proportional to the square of the intensity of the exciting radiation. At the centre of the dye cell the intensities of the two pulses add to enhance the fluorescence. The fluorescence intensity photographed at a distance Z from the midpoint of the dye cell is given by [2.18]

$$I(\tau)=A\left[\int_{-\infty}^{+\infty} I(t)^2\,dt+2\int_{-\infty}^{+\infty} I(t)I(t+\tau)\,dt\right] \tag{2.14}$$

where A is a constant of proportionality and $\tau=2Z/c$. In deriving this relation, time averaging by the photographic process and spatial averaging over several optical wavelengths are assumed. This pulse duration measurement technique has the advantage of directly relating the spatial distribution of the fluorescence to the second-order correlation function $G^2(\tau)$. Eq. (2.14) can be rewritten as

$$I(\tau)=A\left[G^2(0)+2G^2(\tau)\right] \tag{2.15}$$

$$\text{with } G^2(\tau)=\int_{-\infty}^{+\infty} I(t)I(t+\tau)\,dt. \tag{2.16}$$

The complete pulse autocorrelation profile is therefore displayed simultaneously as a function of distance. Since $G^2(\tau)$ becomes zero away from the region of overlap, it is easy to see that the peak to background contrast ratio R of the two-photon fluorescence (TPF) pattern, which is given by

$$R\equiv I(0)/I(\infty) \tag{2.17}$$

has the value 3. When the laser radiation is not a series of single, isolated pulses, but is simply a burst of narrow-bandwidth radiation noise, there will still be a peak at $\tau=0$ in the TPF pattern, due to the overlap of individual

fluctuations with themselves. It has been shown [2.19, 20] that for noise fluctuations the contrast ratio has the value 1.5. For a short burst of noise (*not* a single transform limited pulse) while the peak to background contrast ratio is 3:1, the TPF pattern has a broad base representing the total duration of the burst, with a fine "noise spike" superimposed. Fig. 2.4 was obtained from the first photographs [2.21] of TPF profiles showing this feature. In these experiments the width of the fine spike varied from 0.2 ps to 1 ps but was always correlated with the simultaneously recorded neodymium:glass laser spectral widths of 150 Å to 30 Å. TPF records of single pulses of durations 3 ps, with the theoretical contrast ratio of 3:1, were also recorded (see also Chapt. 3).

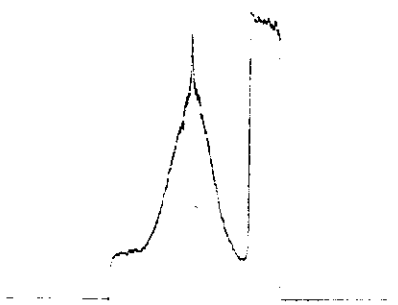

Fig. 2.4. Microdensitometer trace of the TPF pattern obtained from a mode-locked Nd:glass laser (*Bradley* et al. [2.21]). The step on the right indicates a contrast ratio of 2.6. The width of the fine spectral spike is ~0.2 ps

Early reports of subpicosecond pulses from neodymium:glass lasers and of ~5 ps pulses from ruby lasers were based upon TPF patterns, in which only the noise spike was measured. Unfortunately, this led to overoptimistic expectations for the use of these lasers in experiments involving the measurement of picosecond phenomena. The situation was further complicated by the effect of fluorescence quenching under excitation by intense laser radiation [2.22, 23], which leads to a reversal of the TPF "noise spike". Moreover, the nonlinear TPF display technique does not uniquely define the shape of the laser pulse, and the presence of a substantial proportion of the laser energy outside the ultrashort pulses may not be detected. Finally, low intensity pulses cannot be measured. These defects have been overcome by the development of direct photoelectric picosecond chronoscopy with electron-optical streak cameras.

Electron-Optical Picosecond Chronoscopy

The method of studying rapidly varying luminous phenomena by electron-optical chronoscopy was first proposed in 1956 by *Zavoiskii* and *Fanchenko* [2.15], who pointed out that the time resolution of an image tube streak camera is ultimately limited by the spread of the photoelectron transit times in the first image tube. This spread arises from variations in the initial velocities of

the photoelectrons and is mainly developed close to the photocathode, where the photoelectrons are moving slowly, but for x-ray and xuv tubes, and in subpicosecond operation at longer wavelengths, significant time dispersion occurs throughout the photoelectron path (see below).

Photoelectron time dispersion in the image tubes available for use in high-speed streak cameras up to 1970 limited the time resolution to greater than 50 ps. Problems also arose from image distortion and loss of spatial resolution resulting from high photocurrent densities inside the streak tubes [2.24] and it was not clear if picosecond imaging could be obtained. In 1969, picosecond exposures without image distortion were obtained with a gated four-stage cascade image intensifier tube by *Bradley*, et al. [2.25] and the same year it was realised by *Bradley* [2.26] that this time-dispersion limitation could be overcome by the simple expedient of locating a planar, fine-mesh, high-potential electrode close to the tube photocathode. With an otherwise standard streak tube altered in this manner, time resolution was improved to ~5 ps, employing second-harmonic pulses generated by a modelocked Nd:glass laser as test sources [2.27]. Soon after, by applying 20 ns high voltage pulses to the shutter grid of a conventional RCA streak image tube, with a S-1 photocathode. *Schelev* et al. [2.28] measured the durations of the ~10 ps pulses from a Nd:glass laser.

Photoelectron Time Dispersion. Time dispersion occurs over the whole of the photoelectron pathlength in an electron-optical streak tube (Fig. 2.5). The time taken for a photoelectron of initial energy eV_0 in electron volts, emitted normal to the photocathode, to travel a distance x along the tube axis is given by

$$t=(m/2e)^{\frac{1}{2}}\int[V_0+V(x)]^{-\frac{1}{2}}dx. \tag{2.18}$$

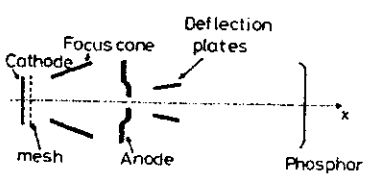

Fig. 2.5. Electrode arrangement and photoelectron transit-time dispersion in electron-optical streak image tube. Photoelectron transit-time to deflection plates is

$$t=\left(\frac{m}{2e}\right)^{\frac{1}{2}}\int_{\text{cathode}}^{\text{plates}}\{V_0+V(x)\}^{-\frac{1}{2}}dx$$

where

V_0 initial photoelectron energy
$V(x)$ axial potential distribution of tube

$V(x)$ is the axial potential distribution for the tube and e and m are the electronic charge and mass, respectively. If $V(x)$ varies linearly with distance x from the photocathode, then (2.18) can be written as

$$t=(m/2e)^{\frac{1}{2}}[(V_0+V)^{\frac{1}{2}}-V_0^{\frac{1}{2}}]E^{-1}. \tag{2.19}$$

E is the uniform axial electric field strength and t is now the time taken to reach a point of potential V. When $V_0 \simeq \Delta V_0 \ll V$ (which is true for all systems employed to date) the well-known result for the dispersion spread of the transit times Δt_D for a spread in initial energies $e\Delta V_0$

$$\Delta t_D \cong (m\Delta V_0/2e)^{\frac{1}{2}}E^{-1}, \tag{2.20a}$$

is obtained [2.13]. Expressing the initial photoelectron energy spread in terms of velocity ΔU, (2.20a) can also be written as

$$\Delta t_D = m\Delta U/eE. \tag{2.20b}$$

The electric field strength E near the photocathode must clearly be maximized so that the transit time spread is minimized, since the quicker the electrons

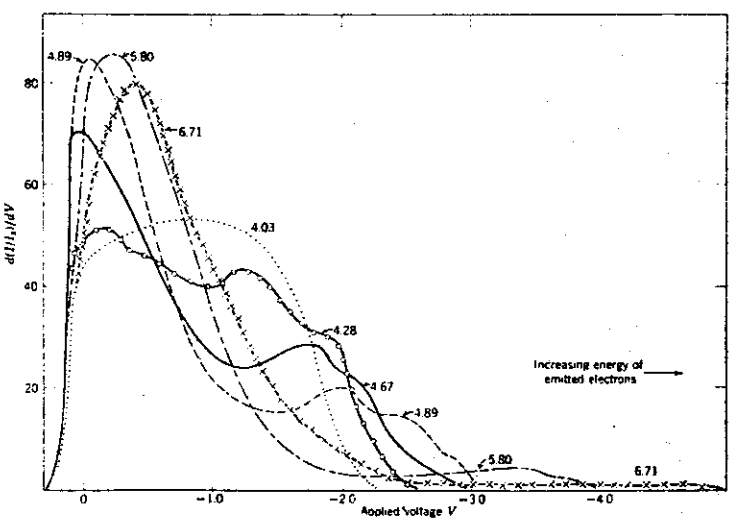

Fig. 2.6. Energy distribution of photoelectrons emmitted by Cs_3Sb photocathode for different photon energies (numbers labelling the curves are in eV) (from *Bradley* [2.56])

are accelerated to a high velocity, the faster they "forget" their small initial differences in energy. The value of ΔU for a particular photocathode depends on the wavelength of the illuminating light. As an example, for an S1 photocathode and 1060 nm light (the wavelength of the Nd:glass laser) the spread in photoelectron energies has a half-width of ~ 0.3 eV, leading to a value of 2.3×10^7 cm s^{-1} for ΔU. To obtain a time resolution of 1 ps in this case requires a photocathode extraction field $E = 13$ kV cm^{-1}. For light of wavelength 600 nm the energy spread is ~ 1 eV so that the time resolution limit at this wavelength is increased to ~ 2 ps for the same photocathode extraction field. Energy spreads of up to ~ 2 eV are produced by other photocathodes with uv illumination (Fig. 2.6). The ultimate time resolution of a streak camera then depends both on the type of photocathode and the wavelength of the light, as well as on the extraction field strength. Thus to construct a camera with picosecond time resolution throughout the spectrum from the vuv to the near ir, extraction fields in the region of 20 kV cm^{-1} were needed. This performance was first demonstrated with the second-generation Photochron II streak tube [2.29, 30] which also has subpicosecond resolution in selected wavelength regions depending upon the photocathode type.

Streak-Camera Systems. The essential components of a streak-camera system and the experimental arrangement used for testing its performance are shown in Figs. 2.7 and 2.8, respectively. The availability of frequency-tunable mode-locked dye lasers [2.31] capable of reliably producing pulses of durations ≤ 2 ps permitted the direct measurement of the resolution of the new streak

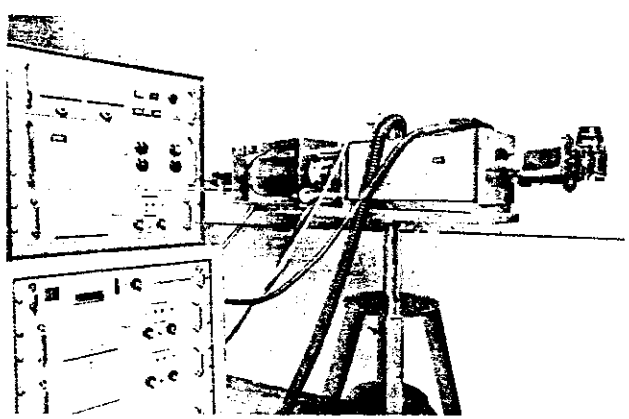

Fig. 2.7. Photograph of Photocron streak camera showing the power supplies, the streak-tube mounting, the four-stage magnetically focused image intensifier and the recording camera

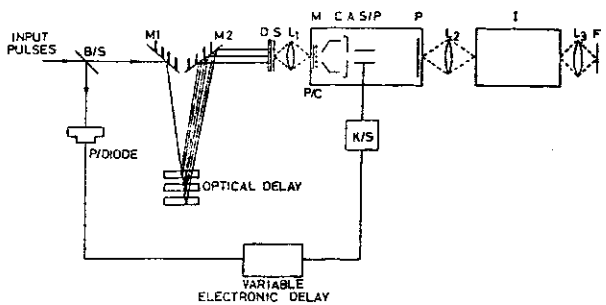

Fig. 2.8. Experimental arrangement for measuring picosecond pulse durations with the Photochron streak camera (from *Bradley* [2.56]) ~~see page 100 for Fig. 2.9~~

tubes [2.32]. An optical delay line arranged (Fig. 2.8) to produce, from a single laser pulse, a series of identical pulses with appropriate separations greatly facilitates calibration of the streak timescale. After an appropriate, variable, electronic delay, the photodiode pulse triggers the krytron circuit, which generates the streak deflection voltage ramp. For a streak length of 5 cm a deflection voltage of 1.5 kV is required. Writing speeds (at the streak-tube phosphor) of $> 2 \times 10^{10}$ cm^{-1} with a jitter of ± 50 ps can be obtained (Fig. 2.9).

Fig. 2.10 shows a typical streak photograph. From microdensitometer traces, such as that of Fig. 2.11, recorded pulsewidths, incorporating both camera response time and laser pulsewidth, as short as 1.5 ps were obtained, thus confirming the subpicosecond resolution capability of the camera. To a good approximation the recorded pulsewidth may be expressed as

$$\Delta t_R = \sqrt{(\Delta t_s)^2 + (\Delta t_D)^2 + (\Delta t_P)^2} \tag{2.21}$$

where Δt_s is the time resolution limit arising from the finite spatial resolution of the overall streak-camera electron-optical and optical systems at a particular streak writing speed, and Δt_P is the laser pulse duration. Normally, the slit-width is set so that its effect on the spatial resolution is negligible. Substituting (2.20b) in (2.21) yields

$$\Delta t_R = [(\Delta t_s)^2 + (\Delta t_P)^2 + k^2 E^{-2}]^{\frac{1}{2}} \tag{2.22}$$

where $k = m\Delta U/e$. In the first experiments with a picosecond streak camera it was confirmed that Δt_R depended linearly on E^{-2} [2.27] and that Δt_D was a linear function of E^{-1}.

As an example the use of (2.21), in the first measurements to directly demonstrate subpicosecond time resolution [2.30] with the experimental arrange-

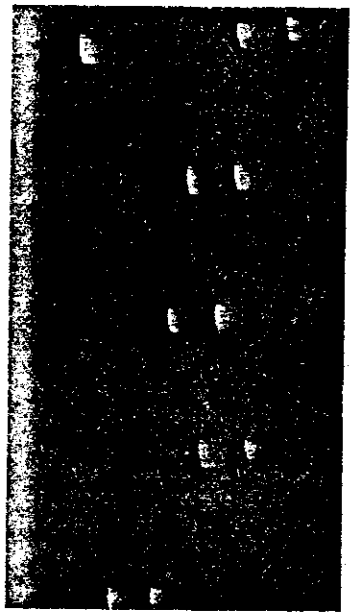

Fig. 2.9. Successive recordings of streaks of pulses from flashlamp-pumped modelocked dye laser showing jitter of ~50 ps. In each streak record the pair of pulses (generated from a single pulse by reflection from the two faces of an optical flat of appropriate thickness) has a separation of 60 ps

ment shown in Fig. 2.12, will be described in some detail. Six pulses from the centre of the pulse train from a rhodamine 6G dye laser, modelocked by DQOCI, were selected out by a Pockels cell optical-switch and amplified to peak powers of ~300 MW. After amplification the pulses were focused into a Raman cell containing ethanol. Transient stimulated Raman scattering from the C–H stretching vibration generates a Stokes frequency at 733.7 nm. The transverse relaxation time of this vibration is ~0.3 ps, and for a laser pulse of duration ~1.5 ps the Stokes pulse generated close to threshold power conditions is shortened [2.34]. The Raman Stokes pulses were transmitted through filters to remove the dye-laser pumping pulses, and two pulses separated by 60 ps were generated from each Raman pulse by reflection from a quartz plate. From the microdensitometer trace (Fig. 2.13) a total recorded duration of 900 fs (900×10^{-15} s) was measured. For pulses of durations as short as this, significant time dispersion occurs outside the photocathode to the mesh region of the streak tube and it is no longer sufficient to employ the approximation of (2.20b) in deriving the time resolution of the camera. Instead (2.20a) must be used to calculate the dispersion over the total photoelectron pathlength from photocathode to anode [2.35]. At a wavelength of 733.7 nm the time-

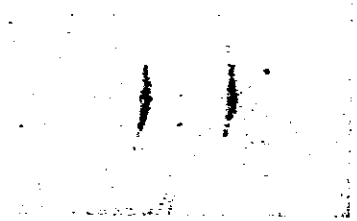

Fig. 2.10. Streak photograph, taken with Photocron II camera, of two pulses separated by 60 ps generated from a pulse (λ 605 nm) from a rhodamine 6G dye laser modelocked by DODCI (from *Bradley* [2.56])

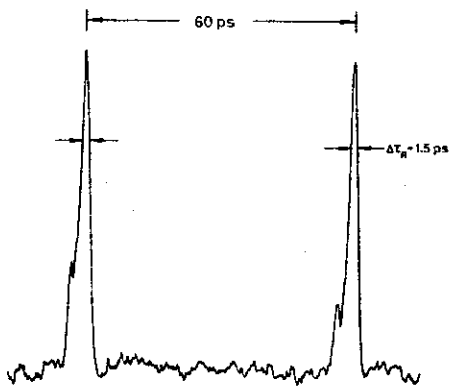

Fig. 2.11. Microdensitometer trace (linear optical density) of a pair of streak images of a pulse (λ 605 nm) from a flashlamp-pumped rhodamine 6G dye laser modelocked by ~~DQOCT~~, demonstrating a total recorded pulse duration of 1.5 ps and confirming the subpicosecond time-resolution limit of the streak camera (from *Bradley* [2.56])

DQOCI

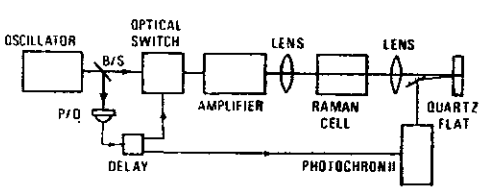

Fig. 2.12. Block diagram of arrangement for generation of subpicosecond pulses by transient Raman scattering in ethanol of 300 MW picosecond pulses from rhodamine 6G dye laser oscillator-amplifier system

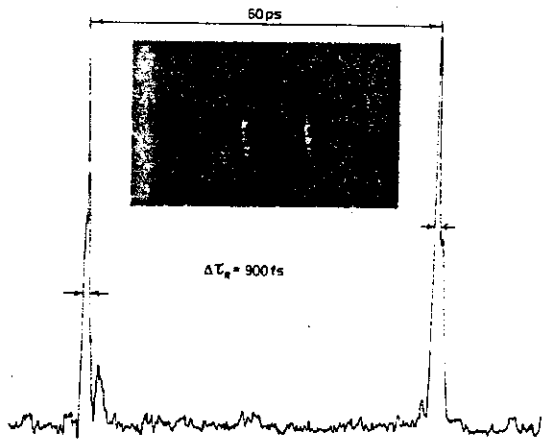

Fig. 2.13. Streak photograph and corresponding microdensitometer trace (arbitrary linear density scale) of Raman-Stokes pulses at 733.7 nm showing recorded half-width of 900 fs

dispersion spread between the photocathode and the mesh is 380 fs, and time dispersion in the mesh to anode region of the tube adds 120 fs, to give a total time-dispersion resolution limit of 500 fs. At a phosphor-screen writing speed of 2×10^{10} cm s^{-1} and with a dynamic spatial resolution of better than 10 line pairs/mm a total camera instrumental resolution of 700 fs is obtained. Using (2.21) to deconvolve this value from the measured pulsewidth of 900 fs gives a Raman pulse duration of 570 fs.

Other picosecond streak-camera systems have recently been developed in the USSR. *Basov* et al. [2.36] and *Fanchenko* and *Frolov* [2.37] employed the newly developed "Picochron" streak camera also to study the structure of the pulses from a modelocked Nd:glass laser. By adding an extra electrostatic lens, an electric field strength of up to 6 kV cm^{-1} at the photocathode is produced in the "Picochron" image tube, giving a limiting time resolution of ~2 ps. An x-band resonance-cavity deflection system continuously sweeps a point image along an elliptical path on the output phosphor. While the resulting total recording time of 15 to 20 ns simplifies sweep timing and synchronisation problems, the use of a point image instead of a slit image seriously reduces the information content per time-resolution element. The facility for picosecond time-resolved spectroscopy or source spatial variation studies is also obviously lost. Another design of slit-streak image tube based on the fine-mesh accelerating electrode principle of the Photochron tubes was introduced in 1972 [2.38] with an electric field strength near the photocathode up to 60 kV cm^{-1} and an experimentally demonstrated time resolution of ~1 ps.

With a new deflection electrode arrangement, the deflection sensitivity was improved to become comparable with that of the Photochron tubes so as to achieve subpicosecond resolution [2.39].

xuv and x-ray Streak Cameras. The study of high-density, high-temperature plasmas for laser fusion [2.40] and the development of coherent light sources in the vuv and xuv [2.41–43] spectral regions require the extension of electron-optical chronoscopy to these shorter wavelengths, with temporal resolution in the picosecond range. This has been achieved by employing gold photocathodes in tubes developed for operation at longer wavelengths. The first camera systems had photocathodes operating with front-surface emission [2.45] and in the transmission mode [2.46–48]. The measured time-resolution limits of these devices were restricted to 60–150 ps by the durations of the laser plasma x-ray pulses employed as test sources. Later experiments [2.35] with short-pulse x-ray emissions produced by 10 ps pulses from a Nd:glass laser demonstrated structures as short as 20 ps. The experimental arrangement is shown in Fig. 2.14. A single pulse from a modelocked laser oscillator was intensity divided by reflection from a double-mirror configuration to give multiple pulses of variable but known separation. When amplified up to energies of ~100 mJ these pulses were focused successively on to a plane copper target to generate a plasma of diameter 100 μm, emitting recombination continua and line radiation up to photon energies of ~1 keV. x-rays in a broad band of energy around 1 keV, selected by an Al foil filter, passed through a tapered slit of width varying from 7 μm to 57 μm to project a magnified shadowgraph image of the slit into the gold photocathode of the streak tube, at a glancing

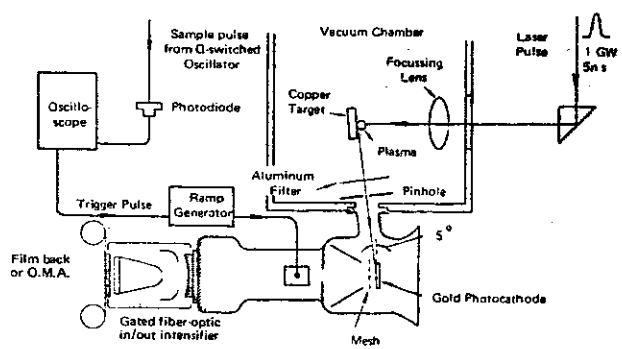

Fig. 2.14. Schematic diagram of x-ray streak camera and laser plasma target chamber. (1) Focusing lens, 12 cm / 3 (2) plane Cu target (3) plasma x-ray source (4) Al filter (5) tapered slit (6) gold photocathode (7) accelerating mesh (8) phosphor screen (9) photodiode (10) streak deflection plates (from *Bradley* et al. [2.35])

angle of 5 . The use of the tapered slit gave a continuously varying photographic exposure. The photocathode field strength was 6 kV cm^{-1} and streak writing speeds of up to 2×10^9 cm s^{-1} were used. Fig. 2.15 is a x-ray streak photograph when the incident laser pulses were separated by 66 ps and the clear resolution is evident from the 70% depth of modulation of the corresponding microdensitometer trace. The shortest recorded pulsewidths were 22 ps. Because of the relatively large energies of the photoelectrons ejected by x-rays there is an associated large spread in photoelectron energy. Using (2.18) the total transit time spread for photoelectrons emitted with different initial energies up to 1 keV was calculated, employing an approximate axial

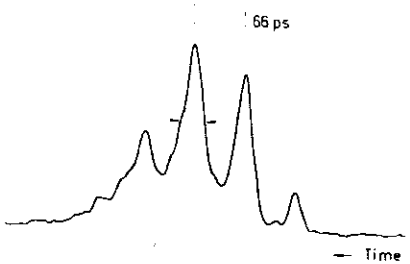

Fig. 2.15a and b. (a) Streak photograph of x-ray pulses generated by the arrangement of Fig. 2.14 when the laser seperation was 66 ps. (b) Microdensitometer trace (linear density scale) of (a). Arrows indicate the half peak intensity level

distribution of the streak-tube potential. Since, from (2.19), the recorded pulse duration will depend upon the value of E and hence on the mesh potential, streak records were obtained for various values of this potential. Knowing the spatial resolution contribution to the recorded pulsewidth, the residual pulse duration, $[(\Delta t_p)^2 + (\Delta t_s)^2]^{\frac{1}{2}}$, was calculated and the best fit to the experimental points was obtained for $eV_0 = 60$ eV, $e\Delta V_0 = 30$ eV and $\Delta t_p = 25$ ps. Then the time dispersion in the photocathode-mesh region amounts to ~ 8 ps, whereas the total dispersion in the tube is 20 ps. Recent direct measurements [2.44] of the photoelectron energy distribution for a gold photocathode irradiated by 1.5 keV x-rays gave the values $eV_0 = 1.1$ eV and $e\Delta V_0 = 3.8$ eV for the secondary photoelectrons. These values would indicate a dispersion-limited time resolution of ~ 6 ps for the tube of [2.35].

These results emphasize the need to properly evaluate all contributions to time dispersion in x-ray and xuv streak cameras when estimating the time resolution limit. Otherwise a too optimistic estimate may be obtained [2.47, 48]. In a recently developed x-ray streak camera the buildup of time dispersion has been considerably reduced by employing a proximity-focused image tube [2.49]. A microchannel plate operates both as an accelerating mesh electrode (to eliminate time dispersion close to the photocathode as in the Photochron tubes) and as a passive collimator, (to replace the usual electrostatic focusing lens). The overall tube length is considerably reduced and the calculated time-resolution limit is ~ 3 ps. Similar results, but with higher spatial resolution should be achievable with magnetically focused tubes [2.50].

Recent technical improvements in picosecond streak cameras include the use of microchannel image intensifiers and fibre-optical coupling (Fig. 2.16) to increase the overall system gain and to provide a more compact and versatile instrument [2.51, 52]. The replacement of photography by optical multi-

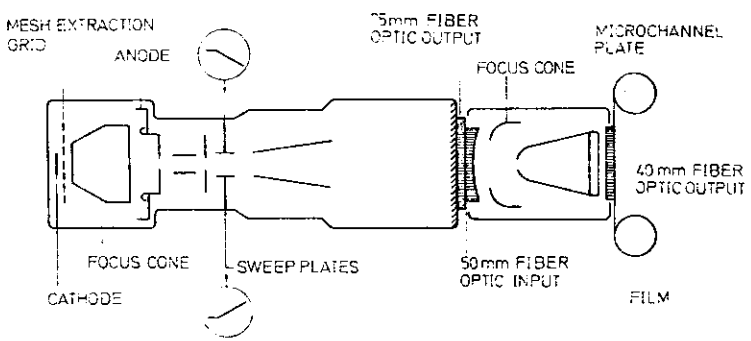

Fig. 2.16. Details of picosecond streak camera system employing fibre-optical coupling (Imacon 675 and 675 II models, Hadland Photonics Ltd.), based upon the Photocron streak tube

channel analysers gives an immediate linear digital record of $I(t)$ [2.53, 54]. The shortest subpicosecond pulses are obtained from cw modelocked dye lasers (see *Modelocked cw Dye Lasers*) with peak powers of 10^2 to 10^3 W. While streak cameras are capable of recording these pulses directly, for studies, for example, of the fluorescence generated repeatedly by such pulses, synchroscan operation of the streak camera [2.55] permits the accumulation of time-resolved data. In this mode of operation the streak plate deflecting voltage is driven synchronously at the repetition frequency (~ 100 MHz) of the modelocked pulse train, so that successive streaks are superimposed on the tube phosphor. The use of digital recording and storage then promises a very convenient system for the study of repetitive phenomena at low light levels. Instrumentation for electron-optical picosecond chronoscopy is still developing very rapidly [2.56]. However with direct linear recording, not only of laser pulses but also of luminous phenomena, over a wide range of photon energies from 1 eV to 10 keV with picosecond time resolution or better, it is clear that a major revolution in chronoscopy has already taken place.

2.2 Types of Modelocked Lasers

The various laser systems with which picosecond pulses have been reliably produced can be divided into two main classes: *i*) giant pulse lasers, such as Nd:glass and ruby lasers, and *ii*) continuous, or quasi-continuous systems, of which the dye laser is the outstanding example.

2.2.1 Giant-Pulse Lasers

Picosecond pulses were first obtained from ruby [2.1] and Nd:glass [2.2] lasers, Q-switched and modelocked by saturable-absorber dye solutions inside the laser resonators. The evolution of ultrashort pulses in these lasers has since been extensively studied both theoretically and experimentally. A typical experimental arrangement is shown in Fig. 2.17. Investigations have shown that the following conditions are necessary to achieve reliable modelocking in giant-pulse lasers.

i) Thermal distortion in the laser rod should be minimized or corrected for, and the laser should operate in a low order transverse mode. These conditions are achieved by employing a spherical mirror with an ancillary corrector lens to produce a generalised confocal cavity [2.57–59] or by filtering the pump light to reduce thermal distortion [2.60]. In either case an intracavity aperture is used to control the transverse mode structure.

ii) Spurious reflections inside the laser resonator and feedback from outside surfaces should be avoided. This is achieved either with a Brewster-angled laser rod and wedged resonator components or with antireflection coatings [2.18, 21, 61]. Outside the cavity lenses of long focal length are useful in isolating other experimental equipment from the laser oscillator [2.62].

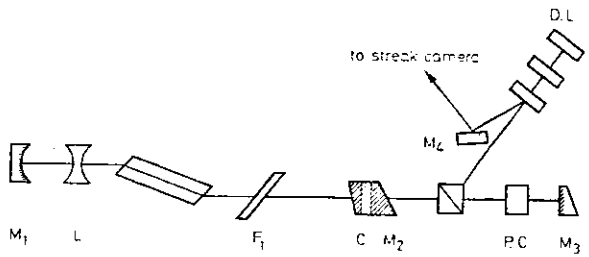

Fig. 2.17. Passively modelocked Nd:glass oscillator. L = thermal distortion corrector lens. C = optically contacted saturable-absorber cell. PC = pockels cell. D.L. = optical delay line. F_1 = flashlamp light filter (from *Bradley* and *Sibett* [2.58])

iii) The saturable absorber dye should be contained in a thin cell in optical contact with one of the laser mirror surfaces [2.60, 62].

iv) The laser should be operated close to threshold and at a high value ($\gtrsim 70\%$) for the low light level transmission of the absorber cell [2.58, 59, 63].

Because of the intrinsic randomness of the passive modelocking process, a completely modelocked pulse train is not produced with a success rate much in excess of $\sim 80\%$ even with these precautions, particularly in the case of the broad-bandwidth, inhomogeneously broadened Nd:glass laser.

It is now well known [2.58, 59, 60, 64] how the shape and duration of the ultrashort pulses generated by a modelocked Nd:glass laser vary along a pulse train. At the beginning of a train the pulses have smooth intensity profiles and durations of 4 to 10 ps. When special care is taken [2.58, 60] bandwidth-limited pulses of 3 to 4 ps are obtained at the beginning of the train. As an example, Fig. 2.18 shows the distributions of pulse durations at two points of the trains emitted by the arrangement of Fig. 2.17. In this system the saturable absorber dye (Eastman Kodak 9860 in dichlorethane) was contained in a cell in contact with the 70% reflectivity plane mirror M_2. (Low light level transmission of the cell was 70%). About ten pulses were switched out of the train by a Pockels cell shutter PC and particular pulses within this group were studied with the streak camera. When the fifth pulse of the train was streaked, pulse durations of 3 to 5 ps were consistently obtained for an absorber dye cell thickness of 50 μm. The streak photograph of Fig. 2.19 shows two images of a single pulse obtained by employing an optical delay line (D.L. of Fig. 2.17) to subdivide each pulse into multiple pulses of predetermined separations. The microdensitometer trace shows a clear separation, as expected from the ~ 2 ps time resolution of the camera. The limiting value of the time-bandwidth product, $\Delta\nu\Delta t = 0.5$, was obtained for several 3 ps pulses. Similar results were obtained by *von der Linde* [2.60] who used careful TPF measurements of the pulse durations. Both investigations demonstrate the advantage of using an absorber dye cell in contact with a laser mirror for reliable generation of

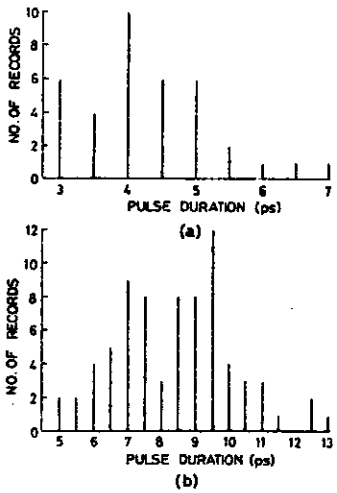

Fig. 2.18a and b. Histogram giving the statistical distribution of the duration of the pulses generated by the modelocked Nd:glass oscillator arrangement of Fig. 2.17 (a) 90 ns from start (10 pulses along train), (b) 500 ns from the start

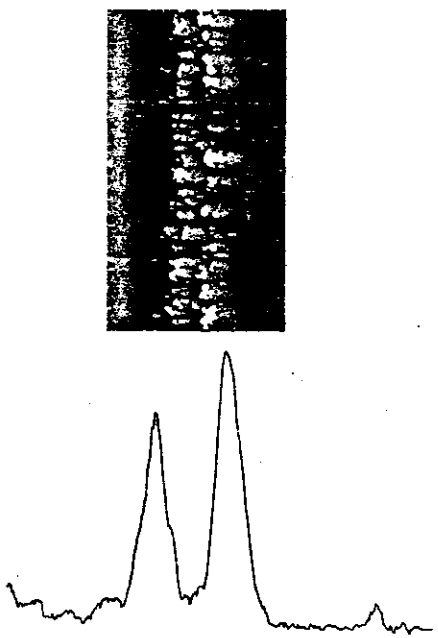

Fig. 2.19. *Top* Streak photograph of two 3 ps pulses, separated by 10 ps, generated in the optical delay line of Fig. 2.17 from a single pulse

Bottom Microdensitometer trace.

ultrashort pulses. The streak-camera measurements also confirmed an earlier report [2.62] that in this mode of operation the shortest pulses are obtained with the shortest dye cell.

Further along the pulse train the spectral bandwidths of the pulses increase rapidly and substructures develop in both the pulse spectra and in the temporal intensity envelopes. This spectral broadening arises from self-phase modulation [2.61, 65–67] caused by the nonlinear interaction of the intense light field with the glass rod. With increasing self-phase modulation the spectral broadening becomes so large that the pulse spectral bandwidth exceeds the amplification bandwidth of the laser material. This results in breakup of the pulse into multiple components, quickly followed by degradation into a burst of noise fluctuations [2.68]. Earlier TPF measurements [2.69] of the cross-correlation of each pulse of a train with its two nearest neighbours had shown that the fluctuation structure of $I(t)$ changed from one round-trip to the next, while the time-integrated autocorrelation function of the whole train exhibited the fine central spike typical of a pulse of random fluctuations (Fig. 2.20). Self-focusing, also arising from the nonlinear refractive index, deviates the radiation out of the laser resonator so that a dip appears in the ultrashort pulse profile [2.70]. Substructure continues to build up as a result of repeated passages through the active medium [2.63, 71]. The effect of self-focusing can also be seen in the oscillogram of the pulse train by a dip in the train envelope, which is characteristic of a well modelocked laser operating at high pulse energies (Fig. 2.21). From the practical point of view these nonlinear effects can be avoided by switching out pulses from the beginning of the pulse train. However, they seriously limit the power density that can be propagated in ultrashort pulse amplifiers. The introduction of a two-photon absorber [2.57, 72] dye cell into the laser cavity greatly reduces the amount of self-focusing. A similar effect has also been obtained by employing intracavity second-harmonic generation [2.73]. In both cases the induced nonlinear absorption limits the

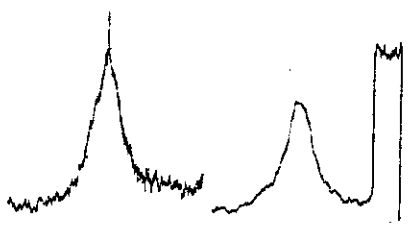

Fig. 2.20. Microdensitometer traces (linear density scale) of the TPF profiles obtained with a modelocked Nd:glass laser. The time-integrated autocorrelation profile (left) of the whole pulse train exhibits the fine central spike similar to that of Fig. 2.4. The spike does not appear in the cross-correlation profile (right) indicating that the pulse temporal substructure changes from one round trip to the next (from *Bradley* et al. [2.62])

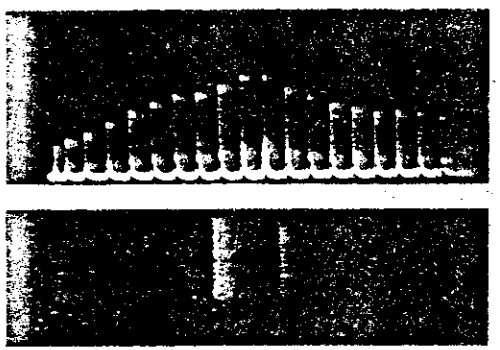

Fig. 2.21. *Top* Oscillogram of modelocked pulse train from Nd:glass laser showing dip in intensity due to self-focusing effects. *Bottom* Streak-camera record of pulse from the beginning of the train before self-action effects arise

peak pulse intensity, leading to more reliable modelocking with better spatial properties in the beams.

Similar pulse trains have been obtained by employing the same experimental arrangements with passively modelocked ruby [2.23, 57, 74, 75] and Nd:YAG [2.56, 71, 76, 77] lasers. Because of the narrower fluorescence bandwidths of these materials the pulse durations lie in the range of 15 to 50 ps and, hence, are too long for many interesting scientific applications of ultrashort laser pulses (see later chapters).

Because of variations in pulse duration throughout the train and because of transient effects in many materials, a single pulse must often be selected for measuring accurately rapid processes in materials [2.60]. Single pulse selection [2.57, 78–84] may be accomplished by passing a train of pulses through a Kerr cell or a Pockels cell that has been activated electronically for a short time, in order to change the polarization of only one of the pulses. To generate the high voltages necessary to rotate the polarization in the Pockels cells, a high voltage spark gap or an all electronic circuit may be used [2.30, 84]. To trigger the circuits, a small fraction of the laser beam is diverted, and by adjusting the optical and electronic delay times, a pulse may be slected from any portion of the train. Experimentalists usually choose earlier pulses in the train because of their shorter durations, and cleaner envelopes.

Before discussing the application of the fluctuation model of a passively modelocked laser to giant-pulse systems, the corresponding results obtained with modelocked dye lasers will be described. Measurements on dye laser systems have elucidated more clearly the significance of absorber recovery time and gain saturation in the generation of picosecond pulses by passive modelocking. Comparison between the ruby laser and the cresyl-violet dye

laser, operating at the same wavelength and modelocked by the same saturable absorbers, has proved to be particularly illuminating.

2.2.2 Dye Lasers

Flashlamp Pumped Systems

While ultrashort pulses were first generated in dye lasers by synchronous pumping with pulse trains from modelocked ruby lasers [2.85, 86] and, after second-harmonic generation, Nd:glass lasers [2.87, 88], the shortest pulses were obtained from passively modelocked systems [2.89]. *Schmidt* and *Schafer* [2.90] had shown that the saturable absorber DODCI[1] could be employed to modulate the output intensity profile of a flashlamp-pumped rhodamine 6G dye laser. This result encouraged other workers to attempt to generate picosecond pulses in this manner, particularly since these pulses could be frequency tuned across the broad spectral bandwidths of the laser dyes. Tunable picosecond pulses were obtained with both rhodamine 6G and rhodamine B lasers [2.91] by employing a diffraction grating as one laser resonator reflector, and immersing the output mirror in the DODCI solution. Two-photon fluorescence measurements showed that in these initial experiments pulse durations of ~5 ps were reliably produced. The introduction of interferometric tuning [2.86] permitted the generation of pulses of bandwidth-limited durations, frequency tunable from 580 to 700 nm [2.92, 93] by employing rhodamine and cresyl-violet laser dyes with the appropriate polymethine saturable absorbers. About the same time the development of picosecond streak cameras permitted direct linear measurement of pulse shapes [2.94, 95].

As a result of extensive streak-camera investigations of ultrashort pulse generation in flashlamp-pumped dye lasers [2.96–99] it became apparent that the mechanism of modelocking dye lasers was quite different from that occurring in giant-pulse lasers. Investigations of the modelocking dyes [2.96, 97, 100, 101] also had shown that the saturable absorber recovery time was at least two orders of magnitude longer than the duration of the modelocked dye laser pulses. These experimental results were incorporated in a simple rate-equation theory [2.102, 103] which showed that the combined actions of amplifier and absorber saturation produced the observed rapid pulse compression.

The experimental arrangement now used for modelocked pulsed dye lasers is shown in Fig. 2.22. The laser dye is pumped uniformly by two Xenon flashlamps in a double-elliptical pumping reflector arrangement. About 100 J of stored electrical energy is dissipated by each flashlamp in ~1 μs. The windows of the quarts cell are wedged at 1° and the laser dye is circulated continually through a fine filter and a heat exchanger for cooling. The saturable absorber solution is contained in a cell and is in optical contact with the 100% reflectivity

[1] DODCI = 3,3'-diethyloxadicarbocyanine iodide.

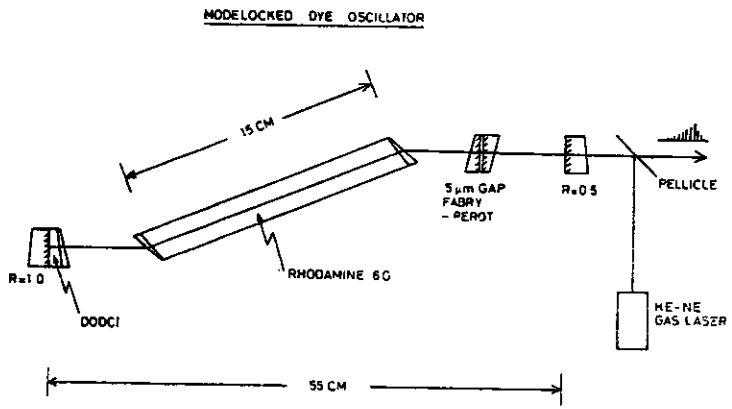

Fig. 2.22. Experimental arrangement for modelocking flashlamp-pumped rhodamine 6G dye laser

mirror. The absorber dye cell window is also wedged at 1°. The lasing dyes are dissolved in water or alcohols, depending upon the operating spectral range required. The laser bandwidth is frequency narrowed and tuned with an intracavity, optically contacted Fabry-Perot etalon of plate separation ~5 μm [2.92. 93]. In this manner transform-limited pulses were first obtained [2.92] over the spectral range 603 to 625 nm (Fig. 2.23). Because of variations in the gain of the active medium and in the absorption of the modelocking dye as the operating wavelength is altered, it is necessary to adjust the saturable absorber concentration for each wavelength to maintain the laser operating just above threshold. The pulse-train envelope also varies with wavelength as can be seen in Fig. 2.24. At the short wavelength end of the tuning range the ultrashort pulse forms very rapidly, whereas at longer wavelengths the output is similar to that of an untuned laser with an initial long pulse buildup section. (Without interferometer tuning the output spectrum of a rhodamine 6G laser modelocked by DODCI shifts to the red (615 nm) and has a bandwidth of ~4 nm [2.92].) Microdensitometer traces of typical, simultaneously recorded, TPF profiles and laser spectra near the extremes of the tuning range are shown in Fig. 2.25. In the absence of frequency modulation (chirping) the laser time-bandwidth product should have the value 0.441 for a gaussian pulse or 0.60 for a lorentzian-shaped pulse. If the modelocked dye laser is operated untuned, or slightly above threshold when tuned, the pulse spectra broaden and develop periodic structures typical of self-phase modulation, as in the case of the solid state lasers. Spectra of pulses selected out from different parts of the modelocked train again showed [2.92] that the spectral broadening increased monotonically along the trains. From these measurements a value for the nonlinear refractive index of the ethanol solvent was deduced.

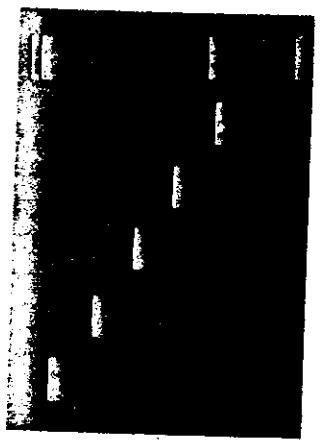

Fig. 2.23. Spectra showing tuning of bandwidth-limited picosecond pulses. Plate of spectrograph was moved vertically as laser was tuned, by rotation of intracavity Fabry-Perot etalon, from 603 nm to 625 nm. Mercury calibration spectrum at top (from *Arthurs* et al. [2.92])

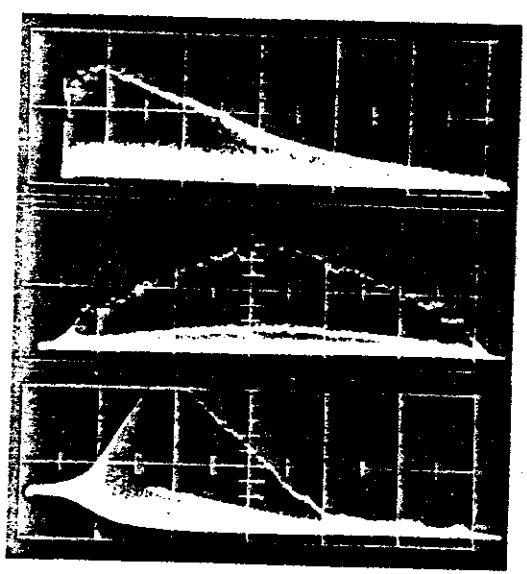

Fig. 2.24. Oscillograms of modelocked pulse trains from etalon tuned Rh 6G laser operating at. *Top* 605 nm. *Middle* 615 nm and *Bottom* 625 nm (from *Roddie* [2.104])

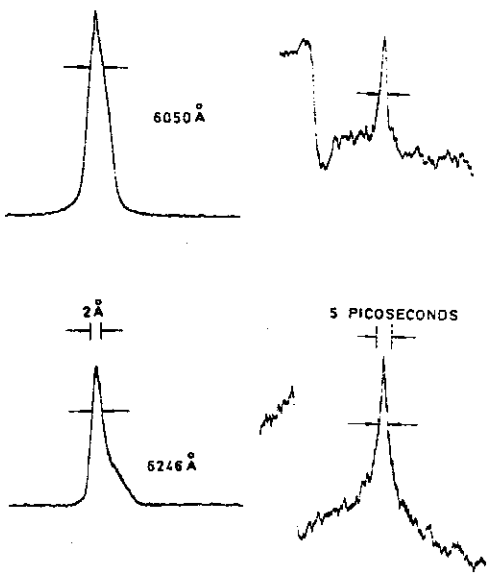

Fig. 2.25. Microdensitometer traces (linear density scale) of two pairs of simultaneously recorded TPF pulses and spectra of bandwidth-limited Rh 6G picosecond pulses (from *Arthurs* et al. [2.92])

The frequency range covered by flashlamp-pumped modelocked dye lasers has since been extended to both shorter and longer wavelengths with the laser dyes and corresponding saturable absorbers listed in Table 2.1. General technical improvements in the dye flow systems, in uniformity of optical pumping, and in laser optical components now permit the routine generation of pulses of a few picoseconds durations or less over the wide range of wavelengths given in the table. Operation of modelocked dye lasers is much less sensitive to variations im pumping energy or to thermal effects in the laser media than is operation of solid state systems. Consequently, the lasers can be used at higher repetition rates, mainly because two strongly nonlinear pulse shortening mechanisms are operating simultaneously and partly because the liquid laser media are more easily kept at uniform temperatures.

Temporal Buildup of Modelocking in Dye Lasers

The paradox that the shortest laser pulses were generated in dye lasers passively modelocked by saturable absorbers of relaxation times of hundreds of picoseconds was cleared up by detailed experimental investigations of the buildup of picosecond pulses [2.96–99, 104, 105]. The nature of the initial buildup

Table 2.1. Picosecond pulse generation in flashlamp-pumped dye lasers

Laser dye	Saturable absorber	Tuning range (nm)	Pulse durations, ps	References
Esculin monohydrate	DASPI	465–480		[1]
Rhodamine 6G	DQOCI	575–600	1.5–3	[2, 3]
	DODCI	600–625	2–3	[3, 4]
Rhodamine B	DQTCI	605–630	3–4	[5]
	DODCI	615–645	2–3	[5, 6]
Cresyl Violet	DTDCI	660–704	3–5	[5, 6, 7]
+ Rhodamine 6G	DDCI	645–680	~3	[5, 6, 7]
	DOTCI	645–680	~4	[5]
DOTCI	HITCCI	795–805		[8]

Dye formulae

DASPI = 2-(P-Dimethylaminostyryl)-pyridylethyl iodide
DQTCI = 1,3'-diethyl-4,5'-quinolythia-carbocyanine iodide
DTDCI = 3,3'-diethyl-2,2'-thiadicarbocyanine iodide
DDCI = 1,1'-diethyl-2,2'-dicarbocyanine iodide
DODCI = 3,3'-diethyl-oxadicarbocyanine iodide
DOTCI = 3,3'-diethyl-2,2'-oxatricarbocyanine iodide
HITCI = 1,3,3,1',3',3'-Hexamethyl-2,2'-indotricarbocyanine iodide
DQOCI = 1,3'-diethyl-4,2'-quinolyoxacarbocyanide iodide

References

1 E.G. Arthurs, D.J. Bradley, T.G. Glynn, A.G. Roddie, W. Sibbett: (unpublished)
2 R.S. Adrain, E.G. Arthurs, D.J. Bradley, A.G. Roddie, J.R. Taylor: Opt. Commun. **12**, 136 (1974)
3 P.R. Bird, D.J. Bradley, W. Sibbett: *Proceedings of 11th International Congress on High Speed Photography* (Chapman and Hall, London 1975), p. 112
4 E.G. Arthurs, D.J. Bradley, A.G. Roddie: Appl. Phys. Lett. **19**, 480 (1971)
5 E.G. Arthurs, D.J. Bradley, A.G. Roddie: Appl. Phys. Lett. **20**, 125 (1972)
6 E.G. Arthurs: PhD Thesis, The Queen's University of Belfast (1972)
7 E.G. Arthurs, D.J. Bradley, P.N. Puntambekar, I.S. Ruddock: Opt. Commun. **12**, 360 (1974)
8 A. Hirth, K. Vollrath, D.J. Lougnot: Opt. Commun. **8**, 318 (1973)

phase was found to depend upon the operating wavelength and the particular saturable absorber employed. For rhodamine 6G modelocked by DODCI and tuned to operate at 605 nm, a very fast buildup of modelocking occurs, and streaks such as that of Fig. 2.26 showed that within a few round trips (20 ns) from the start of the laser action, a fluctuation noise burst of ~100 ps total duration existed in the laser cavity. The subsequent history of evolution to a single picosecond pulse is shown in Fig. 2.27. After ~25 round trips (120 ns) the noise burst has been substantially compressed and then very quickly evolves into a single 2 ps pulse after ~35 round trips. (For calibration purposes two images of each pulse separated by 57 ps were generated in an optical delay line). The very rapid pulse shortening at this wavelength can be clearly

seen in the microdensitometer traces of Fig. 2.28 obtained with the experimental arrangement of Fig. 2.29. By using the pulse delay system two pulses, separated by two round trips, were imaged at different points of the streak-camera slit so as to produce simultaneously separate streak images on a single

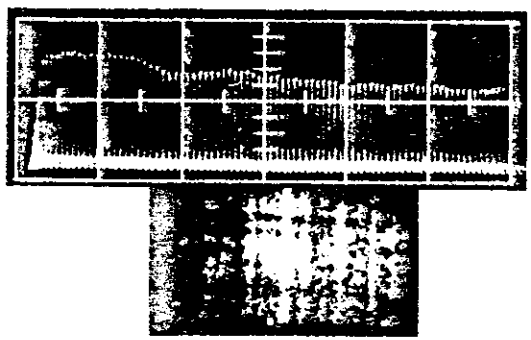

Fig. 2.26. *Top* Oscillogram of the modelocked pulse train of a rhodamine 6G dye laser tuned to operate at 605 nm. Time scale: 50 ns per major division. *Bottom* Streak photograph of fluctuation noise burst "pulse" 20 ns from the start of the pulse train (from *Arthurs* et al. [2.96])

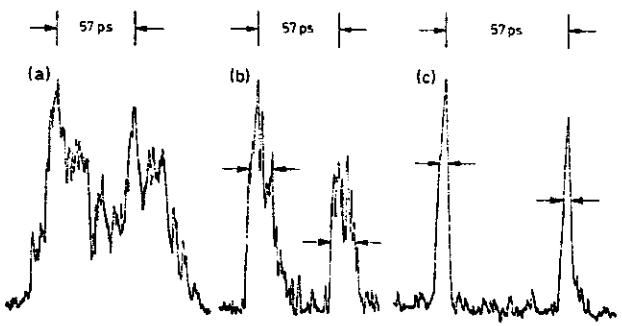

Fig. 2.27a–c. Microdensitometer trace of streak-camera records showing the history of evolution to a single ultrashort pulse in a rhodamine 6G laser modelocked by DODCI. (a) Noise fluctuations at the start of pulse train (b) Halfwidth of envelope of noise pattern reduced to 17 ps after 30 round trips (c) Single 2 ps pulse after 35 round trips. In each case the streak record shows a double pattern generated in the optical delay line from the original pulse so as to provide a known time calibration (from *Adrain* [2.105])

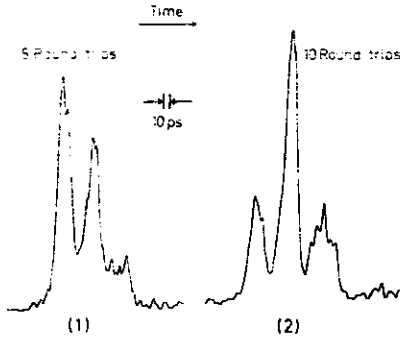

Fig. 2.28. Microdensitometer trace of two simultaneously recorded streak photographs showing pulse evolution in Rh 6G laser. The number of round trips is counted from the start of the pulse train (from *Arthurs* et al. [2.96])

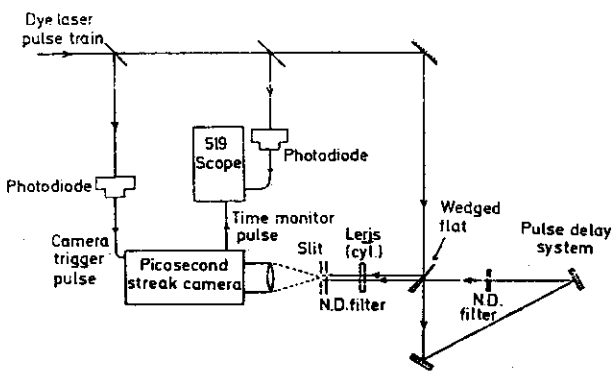

Fig. 2.29. Arrangements for the simultaneous recording of pulse profiles at two different times along the pulse train (see Fig. 2.28)

photograph. The microdensitometer traces[2] show clearly the selectron of a single fluctuation after only two round trips. The fact that the pulse profiles are attenuated at the rear of the envelope as well as at the front demonstrated the important role that saturable amplification played in the passively modelocked dye laser. When the rhodamine 6G laser is tuned to longer wavelengths the pulse buildup takes longer. This behaviour was explained by *New* [2.102] in terms of the wavelength variation of the ratio of the cross sections of the

[2] Since the vertical scale is linear optical density, the smaller fluctuations appear much more intense relative to the pulse peaks.

laser and modelocking dyes. Later studies with the Photochron II streak camera, with subpicosecond time resolution, confirmed that the final pulse duration obtainable was ~2 ps (Fig. 2.10) and that the pulse to background ratio was $>10^4$ implying that >95% of the laser energy was contained within the final isolated picosecond pulse.

Saturable Absorber Recovery Time and Photoisomer Generation. The fact that DODCI is effective as a saturable absorber for modelocking dye lasers operating in the spectral range 584 to 645 nm, although its absorption maximum is at 580 nm, led to the suggestion [2.93] that at longer wavelengths modelocking is due to the generation of a photoisomer, with a ground state lifetime of $\sim 3 \times 10^{-4}$ s and an absorption maximum at 620 nm [2.100]. This photoisomer is generated when DODCI is excited by single-photon, or two-photon [2.57] absorption, giving rise to strong fluorescence peaked at 646 nm. Also, conventional laser-pumped [2.106] and travelling-wave [2.57] DODCI dye lasers operate at ~650 nm. Detailed measurements [2.97] of the fluorescence spectra of both the normal and photoisomer forms of DODCI, with microsecond and picosecond excitation, gave the fluorescence spectra of the photoisomer species (Fig. 2.30).

When the temporal behaviour of the fluorescence from the intracavity absorber cell was monitored at 600 nm and 650 nm with the laser tuned to operate at various wavelengths, the fluorescence at 650 nm initially grew rapidly, relative to the rise of the laser intensity, but then levelled off to follow the laser intensity envelope shape. Likewise the fluorescence at 600 nm fell initially and then also stabilized. The time required for this initial stabilization period was a function of the lasing wavelength. At 607 nm, 100 ns was required by which time a well-defined single modelocked pulse was circulating inside the resonator. For lasing wavelengths longer than 610 nm the attainment of the balance took ~200 ns. It had earlier been found [2.93] that at these wavelengths the modelocked pulses also began to appear after ~200 ns. At wavelengths shorter than 605 nm, where the normal form of DODCI has a large absorption

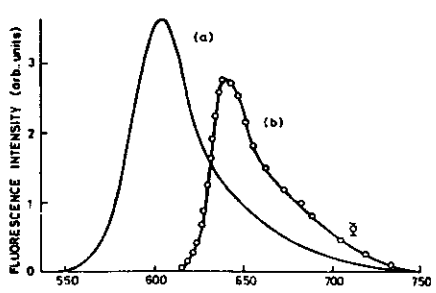

Fig. 2.30. Corrected fluorescence spectra of (a) DODCI recorded on a spectrophotofluorimeter and (b) DODCI photoisomer obtained experimentally (from *Arthurs* et al. [2.97])

cross section, the formation of the photoisomer effectively reduces the dye concentration and this explains why modelocking by DODCI is difficult at these wavelengths.

The excited-state fluorescence lifetimes of the two species of DODCI were measured when the pulse train from a modelocked, rhodamine 6G laser, tuned to 605 nm, was focused into a cell containing the absorber solution. A microdensitometer trace of a typical streak-camera fluorescence time profile is shown in Fig. 2.31. From a large number of such profiles the fluorescence decay time was measured to be 330 ± 40 ps for both the normal and photoisomer species. The decay of the sidelight fluorescence from the intracavity cell was also investigated with the streak camera and the results obtained were identical. However, in the case of the intracavity cell the photoisomer fluorescence was dominant.

The recovery time of the DODCI absorption following intense picosecond excitation was investigated with the experimental arrangements of Fig. 2.32a, b [2.97]. For studying the dye while operating as a saturable absorber *inside* the laser resonator, the modelocked pulse train (Fig. 2.32a) was telescoped up to reduce beam divergence, apertured, and then attenuated by neutral density filters to produce a low intensity uniform beam. After passing through a delay line, a polarizing prism, and further apertures, the beam was arranged to overlap again with the resonator beam inside the DODCI modelocking cell. A micrometer control of the position of the delay line prism permitted timing of the arrival of the pulses of the probe beam to 0.5 ps. The probing pulse train was monitored, before and after transmission through the cell.

Fig. 2.33 shows the transmission at a particular time during the train plotted against the delay of the probing pulse, for the laser operating at ~610 nm. The 1/e recovery time τ_A of the absorption is ~225 ps. Similar

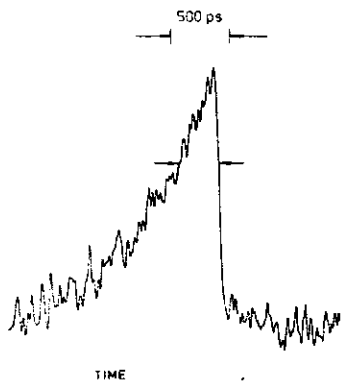

Fig. 2.31. Microdensitometer trace of streak-camera record of DODCI fluorescence time profile under same conditions as inside a modelocking cell in the laser cavity. Corrected e^{-1} decay time is indicated. (Ordinate is linear density scale and the recorded signal to noise ratio is 20:1)

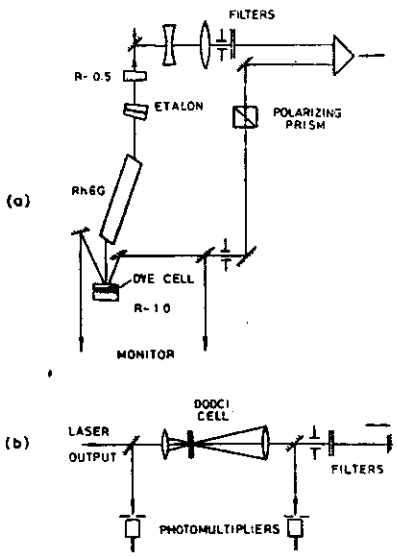

Fig. 2.32a and b. Methods of measuring saturable-absorber recovery time. (a) Inside modelocked dye laser cavity, (b) outside the laser resonator

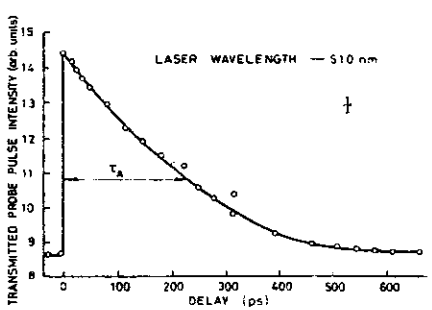

Fig. 2.33. Transmission of intracavity DODCI cell after excitation by a picosecond pulse as measured by arrangement (a) of Fig. 2.32 (from *Arthurs* et al. [2.97])

recovery profiles were obtained for all times during the pulse train, after the evolution of ultrashort pulses, for the laser operating in the range 595 to 620 nm. In all cases, the transmission remained constant over the 3.5 ns period following the absorption recovery until the next exciting pulse entered the cell. The value of this interpulse transmission $T(\infty)$ relative to the low-level transmission T_L of the unexcited DODCI depended on the operating wavelength

of the laser. At wavelengths shorter than ~605 nm, where the photoisomer absorption cross section is larger [2.100] $T(\infty)$ was less than T_L.

The absorption recovery was also measured outside the laser resonator with the arrangement of Fig. 2.25b. The results obtained gave typical values of ~240 ps for τ_A. Assuming an optically thin sample cell, containing a two-level absorber, with spatially uniform excitation, by an intense, delta function pulse, the transmission $T(t)$ of the medium at time t after excitation is given by

$$\text{Ln}\,[T(t)/T(0)] = [1-\exp(-t/\tau_1)]\,\text{Ln}\,[T(\infty)/T(0)] \tag{2.23}$$

where τ_1 is the lifetime of the upper state. This relation shows [2.107] that the aperture time τ_A is strongly dependent upon both $[T(\infty)/T(0)]$ and τ_1. Knowing τ_A, the value $\tau_1 \sim 300$ ps was calculated for particular values of $[T(\infty)/T(0)]$.

Comparison of Modelocked Ruby and Cresyl-Violet Lasers. With the development of the modelocked cresyl-violet laser it was possible [2.98, 99] to directly compare the mechanism of pulse generation in the ruby laser and in a dye laser operating at the same wavelength and each modelocked by saturable absorbers of different molecular relaxation times (Table 2.2).

The ruby laser, operated in a single transverse mode of beam divergence < 1 mrad, produced regular pulse trains of total duration ~250 ns (~100 mJ total energy) when modelocked by DDCI or DTDCI. Both absorbers were contained in a cell of 200 μm thickness in optical contact with the 100% reflectivity spherical mirror [2.108]. With DDCI the pulse durations were in the range 15 to 30 ps but the pulses produced by DTDCI were longer, 90 to 105 ps. In both cases the fluctuation structure near the end of the linear phase of laser amplification develops into a train of isolated single pulses at the start of the giant pulse. More details can be seen in the streak-camera traces. The average duration of the fluctuations in Fig. 2.34a is ~120 ps, in good agreement with the ruby laser bandwidths of ~0.2 Å [2.108] at the end of the linear amplification stage. The selection of the most intense fluctuations and their gradual compression is clearly shown in the later streaks. This pattern of development is typical of solid state lasers modelocked by absorbers of very short relaxation times. The pattern obtained with DTDCI is, on the other hand, very similar to that seen in dye lasers, except that in the case of the ruby laser the final pulse duration is determined by the aperture time of the modelocking DTDCI dye cell, which was measured to be ~120 ps. (The corresponding aperture time for the DDCI cell was 13 ps.) It is interesting to note that the DTDCI cell aperture time equals the shortest fluctuation time in the trace of Fig. 2.34. Since in this case the dye relaxation time is longer, bleaching of the absorption occurs by energy saturation and the absorber tends to select a broad group of fluctuations. In keeping with this picture the final pulse shape measured with the streak camera was asymmetrical with a sharp leading edge.

These results with the ruby laser, showing that the absorber cell aperture time determined the pattern of pulse generation, demonstrated that the two

Table 2.2. Lifetimes (relaxation times) of saturable absorber molecules

Dye	Molecular lifetimes		References
	Absorption	Fluorescence	
DDCI			
In methanol	25 ps	—	[1]
	—	14 ps	[2]
In ethanol	—	11 ps	[3]
DCI (cryptocyanine)			
In methanol	80 ps	—	[4]
	16 ps	—	[5]
	—	110 ps	[6]
	—	20–40 ps	[7]
In ethanol	—	37 ps	[3]
DCI			
In ethanol	10 ps	—	[8]
	—	20 ps	[1]
DTDCI			
In ethanol	175 ps	185 ps	[1]
	—	1.2 ns	[9]
DODCI			
In ethanol	10–250 ps	—	[10, 11]
	1.15 ns	—	[12]
	1.2 ns	—	[13]
	300 ps	—	[14]
	—	420 ps; 1.2 ns	[15]
	—	330 ps	[16]

References

1 E.G. Arthurs, D.J. Bradley, P.N. Puntambekar, I.S. Ruddock, T.J. Glynn: Opt. Commun. 12, 360 (1974)
2 M.A. Duguay, J.W. Hansen: Opt. Commun. 1, 254 (1969)
3 D.N. Dempster, T. Morrow, R. Rankin, G.F. Thompson: Chem. Phys. Lett. 22, 222 (1973)
4 G. Mourou, G. Busca, M.M. Denariez-Roberge: Opt. Commun. 4, 40 (1971)
5 J.P. Fouassier, D.J. Lougnot, J. Faure: Chem. Phys. Lett. 30, 448, (1975)
6 G. Mourou, G. Busca, M.M. Denariez-Roberge: IEEE J. QE-9, 745 (1973)
7 M.A. Duguay, J.W. Hansen: Opt. Commun. 1, 254 (1969)
8 M.W. McGeoch: Opt. Commun. 7, 116 (1973)
9 D.N. Dempster, T. Morrow, R. Rankin, G.F. Thompson: J. Chem. Soc., Faraday II 68, 1479 (1972)
10 G.E. Busch, R.P. Jones, P.M. Rentzepis: Chem. Phys. Lett. 18, 178 (1973)
11 G.E. Busch, K.S. Greve, G.L. Olson, R.P. Jones, P.M. Rentzepis: Chem. Phys. Lett. 33, 412 (1975)
12 D. Madge, M.W. Windsor: Chem. Phys. Lett. 27, 31 (1974)
13 C.V. Shank, E.P. Ippen: Appl. Phys. Lett. 26, 62 (1975)
14 E.G. Arthurs, D.J. Bradley, A.G. Roddie: Opt. Commun. 8, 118 (1973)
15 J.C. Mialocq, A.W. Boyd, J. Jaraudias, J. Sutton: Chem. Phys. Lett. 37, 236 (1976)
16 E.G. Arthurs, D.J. Bradley, A.G. Roddie: Chem. Phys. Lett. 22, 230 (1973)

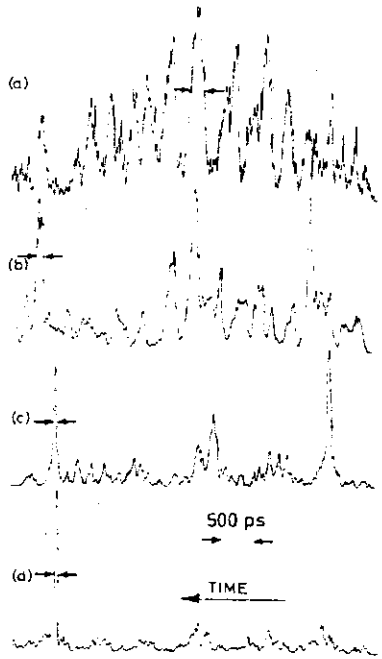

Fig. 2.34 a–d. Sequence of streak camera microdensitometer traces (time resolution ~30 ps) of pulse evolution in ruby laser modelocked by DDCI. (a) 3 μs (b) 2.5 μs (c) 1.5 μs (d) 1 μs before peak of giant pulse, respectively

cases of modelocking dye lasers modelocked commonly met by absorbers of long lifetimes and solid state lasers with short duration absorbers, are special cases. In ruby and Nd:glass lasers the absorber cell aperture time sets a lower limit to the final pulse generated. In the case of dye lasers the very short storage times of the laser media result in the domination of saturable amplification so that picosecond pulses can be generated with saturable absorbers of a very wide range of relaxation times. This analysis was confirmed by studies of modelocking of the cresyl-violet laser [2.98]. The absorption spectra of the modelocking polymethine dyes used are shown in Fig. 2.35. The absorber-cell aperture times were measured by the methods used for DODCI, employing picosecond pulses from the modelocked laser tuned to operate at the appropriate wavelengths. The results obtained are given in Table 2.2 together with the corresponding results obtained by other researchers. The ability of DTDCI to modelock at 694.3 nm arises from the generation of a photoisomer with an absorption spectrum shifted to the red [2.100] as in the case of rhodamine 6G modelocked by DODCI at 625 nm. While there has been controversy [2.101, 109] over the value of the molecular lifetime of DODCI, and even about the

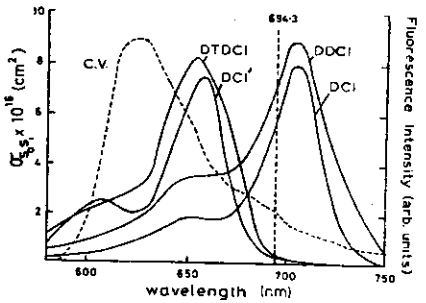

Fig. 2.35. Variation of absorption cross sections of saturable absorbers as a function of wavelength. The fluorescence spectra of cresyl-violet are also shown

existence of the photoisomer [2.110], from the point of view of understanding the modelocking process the relevant recovery time is the shortest *aperture time* of the intracavity saturable absorber dye cell, *under modelocking conditions*. As pointed out by *Mourou* et al. [2.111] care has to be taken in determining the molecular lifetime from absorption relaxation measurements, to correct the aperture time for the particular low light-level transmission used and the induced absorption change. Also stimulated emission can affect the measurements [2.112]. In the cases of DODCI and DTDCI, photoisomer generation adds further complications.

The efficiency of lasing is improved by employing a mixed solution, in ethanol, of rhodamine 6G and cresyl-violet. The longest pulse trains are generated with DTDCI and, in general, the rate of picosecond pulse buildup increases with the gain of the active medium, i.e., as the laser is tuned to shorter wavelengths. Pulse durations of ~4 to 7 ps were consistently obtained at the middle of the train with all of the four modelocking dyes (DTDCI, DDCI, DCI and DCI'). The effect of absorber relaxation time is clearly seen for the two cases in the streak camera records of Fig. 2.36. Traces (b)–(d) for DTDCI modelocking correspond to times 150, 350 and 500 ns, respectively, after lasing threshold was achieved. (Double transit time was 4 ns.) With the broad lasing bandwidth (~3 nm) of the untuned laser the shortest initial fluctuations would have durations of ~200 fs (200×10^{-13} s), so the saturation of the DTDCI absorber would therefore be determined by the integrated energy density. With DDCI and an initial bandwidth of 0.5 nm the streak traces (at times corresponding to 85, 90 and 95 round trips, respectively, after threshold) show an evolutionary process similar to that occurring in the ruby laser modelocked by the same dye (see Fig. 2.34). In the dye laser case a considerably more rapid selection rate arises from the much greater effect of gain depletion.

Modelocked cw *Dye Lasers*

While the continuous working dye laser has been actively modelocked [2.113, 114] the shortest pulses are obtained in passively modelocked systems. Pulses

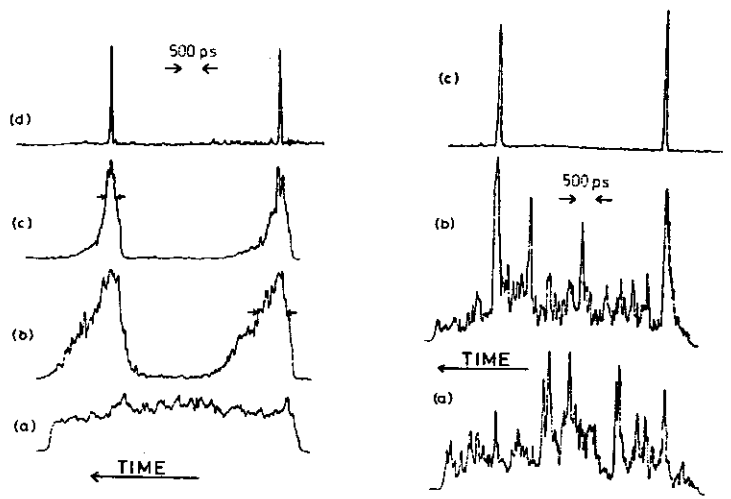

Fig. 2.36. Sequence of streak-camera microdensitometer traces (time resolution ~30 ps) showing ultrashort pulse development in cresyl-violet laser modelocked by (L.H.S.) DTDCI (untuned.) and (R.H.S.) DDCI (tuned to 695 nm) (see text for details)

of durations of a few picoseconds were first obtained from the cw rhodamine 6G dye laser [2.32, 115, 116] passively modelocked by DODCI. Since then, subpicosecond pulses have been obtained by compressing, with a grating pair, the frequency-chirped pulses generated in a system employing two free-flowing dye streams, one for the active medium and one for the absorber, respectively [2.117] (see also Chap. 3). Transform-limited pulses of durations as short as 0.3 ps have been produced [2.118] in the cavity configuration shown in Fig. 2.37, which allows the use of all lines of the Argon-ion laser [2.98]. The saturable-absorber dye flows, in contact with the ~100% broadband reflectivity mirror, in a narrow channel of thickness variable from 200 μm to 500 μm. Both the window and the channel of the absorber dye cell are wedged to 1° to eliminate subcavity resonances. The rhodamine 6G dye laser beam is focused into the absorber solution by a lens so as to increase the power density fourfold. The lens and the cell window are both antireflection coated. The laser dye flows in a jet near the centre of the resonator. Output mirror transmissions from 1 to 6% at 600 nm are employed and the round-trip time varies from 10 ns to 12 ns. With an absorber cell thickness of 0.5 mm pulses of ~1 ps durations are readily obtained. Pulse durations are further reduced to 0.3 ps (at 610 nm) when the DODCI cell length is shortened to 200 μm. Under these conditions the subpicosecond pulses are tunable over the range 598 to 615 nm. Pulse

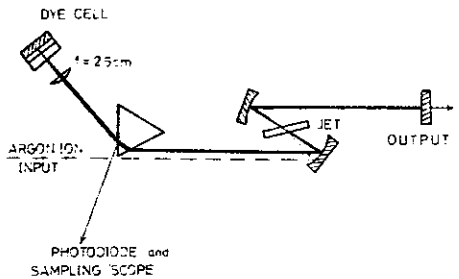

Fig. 2.37. Passively modelocked cw dye laser configuration

duration and stability are not dependent upon pumping level and the dye laser can operate up to 20% above threshold to give an average output power of 15 mW for 0.5 ps pulses (peak power 300 W). When the optically contacted absorber cell was replaced by a second free-flowing dye stream, single pulses were obtained only close to threshold as has been observed by other workers [2.119]. At higher pumping powers structured pulses were produced, as detected both by second-harmonic autocorrelation and streak-camera measurements. Another striking difference lies in the pulse shapes produced by the contacted and free-flowing absorber arrangements. In the former, the best fit to the autocorrelation traces gives a sech^2 pulse shape in good agreement with a recent theoretical model [2.120]. For the noncontacted cell the pulses are characterized by exponential trailing edges. Similar single-sided exponential pulse shapes have been reported by *Ippen* and *Shank* [2.117].

Confirmation of the generation of bandwidth-limited subpicosecond pulses by the narrow-gap contacted absorber cell was given by simultaneous temporal and spectral intensity recordings, such as Fig. 2.38. These pulses, having the high degree of organisation represented in Fig. 2.2b, are particularly valuable for experiments in nonlinear optics because the interpretation of the results is then relatively simple.

As with the flashlamp-pumped rhodamine 6G laser modelocked by DODCI, at wavelengths less than 600 nm modelocking of the cw laser deteriorates due to the decrease in the DODCI photoisomer absorption cross section at these wavelengths. Again, the use of DQOCI extends the range of ultrashort pulse generation in the cw laser to cover the spectral region 580 to 613 nm. Subpicosecond pulses have also been obtained with DQOCI, although detailed investigations of the tuning range have not been carried out. However, it is anticipated that bandwidth-limited subpicosecond pulses will be available over most of the DQOCI modelocking range.

Employing the various combinations of laser dyes and saturable absorbers given in Table 2.3 continuous tuning of the modelocked cw dye laser has been achieved over the range 580 to 630 nm with the optically contacted absorber dye cell arrangement. It is likely that bandwidth-limited pulses of ~100 fs

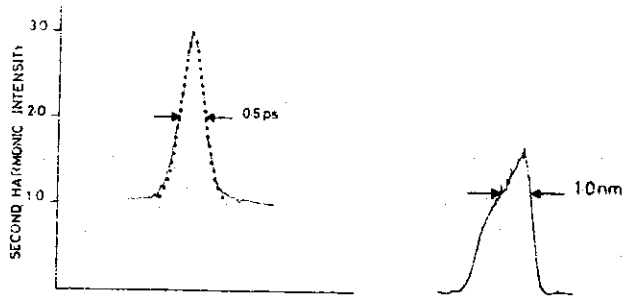

Fig. 2.38a and b. (a) Second-harmonic autocorrelation trace for laser operating at wavelength 607 nm. The discrete points are calculated for a sech^2 laser pulse intensity profile. (b) Microdensitometer trace of the spectrum of modelocked laser recorded simultaneously with the pulse duration measurement of (a). Arrows indicate the spectral halfwidth (linear density scale)

Table 2.3. Continuous wave Dye Lasers Modelocked by Contacted Absorber Dye Cell

Laser dye	Absorber dye	Pulse duration (ps)	Tuning range (nm)
Rhodamine 6G	DODCI	Sub-picosecond	598–615
		0.3[a]–1.5	592–617
	DQOCI	0.6[a]–2	580–613
Rhodamine B	DODCI	3–4	610–630
	DQOCI	4–5	600–620
	Cresyl-violet	3–4	610–620
Sodium fluorescein	Rhodamine 6G	5–7	546

[a] 200 μm cell thickness
(Data from I.S. Ruddock: PhD Thesis, University of London (1976))

durations could be obtained with narrower dye cells and general engineering improvements. There must be a minimum number of optical cycles to define the stationary-pulse sech^2 intensity profile, and because there would be only ~50 cycles in a 100 fs pulse, it is evident that we are approaching the limit for ultrashort pulse generation in the visible region.

Synchronously Pumped Dye Lasers

As mentioned in *Flashlamp Pumped Systems*, the generation of ultrashort pulses in dye lasers was first achieved by pumping with pulse trains from high power modelocked ruby [2.85, 86] and from the second-harmonic of modelocked Nd:glass lasers [2.87, 88]. By setting the cavity length of the dye lasers equal to, or a submultiple of, that of the pumping lasers, the gain of the dye laser was impulsively driven in synchronism with the cavity round-trip repetition

rate, thus producing a train of short duration pulses. The pulses of shortest duration (15 to 20 ps) were obtained from the second-harmonic pulse train of a Nd:glass laser longitudinally pumping rhodamine *B* in a matched 1 m cavity [2.89]. This technique of synchronous pumping by modelocked solid state lasers has recently been taken up again [2.121]. Bandwidth-limited pulses of durations as short as 12 ps have been obtained [2.122, 123] by pumping with second-harmonic pulses from a repetitively pulsed (50 Hz), passively modelocked Nd:YAG laser. The dye laser was spectrally narrowed and tuned by two intracavity Fabry-Perot etalons. When the dye laser cavity length was matched to the pulse separation of the pumping laser train, the dye pulses were generated in time coincidence with, and had durations ($\sim$30 ps) little longer than the pump pulses. By slightly lengthening the dye laser cavity from the matched length (by $\sim$0.8 mm) the resulting gain depletion arising from the increasing delay, with respect to the pumping pulse, of the circulating dye laser pulse, results in a shortening of this pulse by a half. An extensive tuning range of 549 to 727 nm was obtained for synchronous modelocked operation with rhodamine 6G, rhodamine B, cresyl-violet, and carbazine 122 dyes in a variety of solvents. Because of the reduced ground-state absorption in the highly inverted dyes under synchronous pumping, it is possible to tune to shorter wavelengths than in the case of flashlamp-pumped and cw dye lasers. With rhodamine 6G the bandwidth-limited pulses had durations of 12 to 16 ps with peak powers of $\sim$1 MW. These results are to be compared with bandwidth-limited pulse durations of $\sim$2 ps and peak powers of also $\sim$1 MW obtainable from passively modelocked flashlamp-pumped systems [2.92].

Synchronous pumping has also been employed with modelocked argon-ion lasers [2.124–127]. Stable modelocking, to produce bandwidth-limited pulses of $\sim$7 ps duration at a repetition rate of 10^8 Hz, and frequency tunable from 565 to 625 nm, has been obtained [2.128]. The dye laser is pumped by a modelocked argon-ion laser of $\sim$800 mW average power and pulsewidths of 200 ps. The conversion efficiency is $\sim$40% and the resulting dye laser pulses have peak powers of $\sim$500 W (average power 350 mW).

Earlier, *Runge* [2.129] had reported an arrangement in which cresyl-violet, Nile Blue *A* and DTDCI dyes had been employed to passively modelock a He-Ne laser, and were found to lase and to emit a train of pulses with the same repetition rate as the He-Ne laser. By separating out the dye laser and gas laser cavities, DTDCI could be wavelength tuned over a broad spectral region when intracavity pumped in this way by the He-Ne laser [2.130]. Modelocked pulse trains at two frequencies have also been produced when a mixture of rhodamine 6G and cresyl-violet was pumped in the usual cw dye laser configuration by an argon-ion laser [2.131]. At a pump power of 1 W, simultaneously modelocked lasing was observed at the two wavelengths of 574 and 644 nm. However, no pulse duration measurements were reported and at higher pump powers simultaneous cw lasing at the two wavelengths occurred.

Fan and *Gustafson* [2.132] have generated narrow-band picosecond pulses from a rhodamine B dye laser with a cavity length of 50 to 125 μm pumped by frequency-doubled pulses ($\sim$5 ps) from a passively modelocked Nd:glass laser. Pulses of $\sim$3 ps duration with a spectral bandwidth of $\sim$5 Å (time-bandwidth product value of 1.25) were produced with an energy conversion efficiency of up to 40%. The emission wavelength varied from 0.60 to 0.63 μm depending upon dye concentration and cavity length. As pointed out by *Roess* [2.133] a high ratio of pumping pulse duration to cavity lifetime results in laser pulse shortening.

2.3 The Fluctuation Model of Modelocked Lasers

The experimental results, described and discussed in Section 2.2, can be explained for both giant-pulse lasers and dye lasers in terms of the fluctuation model of the passively modelocked laser. This model was first formulated by *Letokhov* [2.134] and, independently, by *Fleck* [2.135, 136], to show how ultrashort pulses are generated in giant-pulse systems from the initial fluorescence intensity fluctuation patterns of the laser media.

2.3.1 Passive Modelocking of Giant-Pulse Lasers

The various stages of evolution of a modelocked pulse are shown in Fig. 2.39. Spontaneous fluorescence emission begins at the start of the flashlamp pumping pulse. As the pumping continues, the gain of the laser medium builds up and the intracavity radiation pattern develops a structure periodic in the round-trip time $T = 2L/c$. When the gain is sufficient to overcome the linear and nonlinear losses in the cavity, laser threshold is achieved and the period of linear amplification begins (at time t_1 in Fig. 2.39). Because of the higher gain at the centre of the lasing bandwidth, spectral narrowing occurs during this stage with consequential increases in the durations of the fluctuations in each round-trip period. In the nonlinear stage of ultrashort pulse development, which begins at time t_2, the random pulse structure is transformed by the combined actions of nonlinear saturation of the absorber and laser gain saturation. As a result, one of the fluctuation spikes grows in intensity until it dominates. This surviving pulse also experiences some shortening in duration and an increase in spectral bandwidth. The important role of laser gain depletion during the nonlinear stage of amplification in producing a strong discrimination of pulse intensities was pointed out by *Glenn* [2.137, 138]. Earlier treatments [2.14] assumed negligible gain saturation. This assumption is in keeping neither with the values of the laser parameters nor with the results of the experimental investigations.

In the nonlinear amplification phase the net gain experienced by a pulse per round trip is given by [2.138]

$$dI_k/dk = I_k[A_k - \Gamma - B_0(1 + I_k)] \tag{2.24}$$

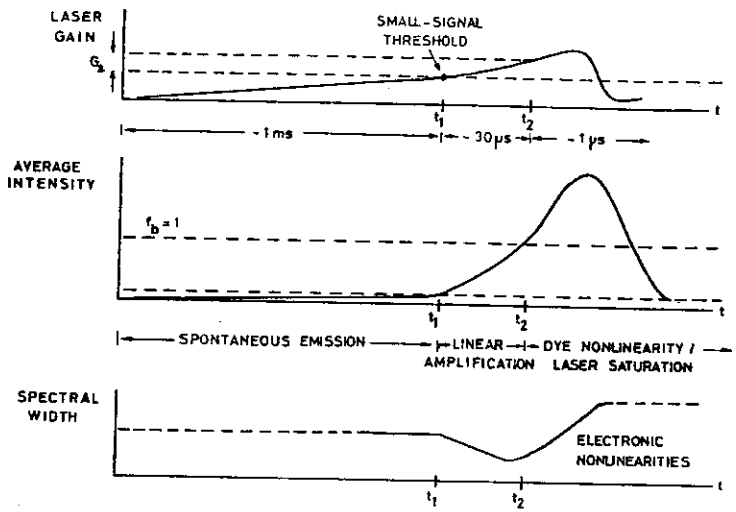

Fig. 2.39. Behaviour of gain, intensity and spectral width of passively modelocked Nd:glass laser (From E.H.C. New unpublished).

where I_k is the pulse intensity at the k-th pass, normalized to the absorber saturation intensity $I_s=(2\sigma_b T_{1b})^{-1}$, A_k is the gain per pass, and Γ represents the cavity losses arising from scattering and the mirror transmissions. σ_b and T_{1b} are the cross section and the relaxation time of the saturable absorber dye, respectively, and B_0 is the initial absorption coefficient. The gain coefficient A_k obeys the equation

$$dA_k/dk = -A_k(2\sigma_a I_s T)I_k + fT \tag{2.25}$$

where f is the rate of flashlamp pumping and σ_a is the gain cross section. In deriving (2.24) and (2.25) it is assumed that the nonlinear absorber has instantaneous response, and that the flashlamp pumping produces a linearly increasing value of A, as shown in Fig. 2.39. The effective gain coefficient is

$$G = A - \Gamma - B_0/(1+I_k). \tag{2.26}$$

At time t_2, G is positive for all the pulses of the circulating intensity pattern. After that time only pulses above the critical intensity, given by

$$I_c = [(B_0/(A-\Gamma)] - 1 = [B_0/(B_0+\Delta A)] - 1 \tag{2.27}$$

for which $G=O$, will continue to grow since as the gain becomes depleted, $\Delta A = A - \Gamma - B_0$, becomes negative.

In the computer simulation model employed by Glenn, the gain was assumed to be constant during a pass through the laser and was recalculated at the end of each pass, taking into account the total energy extracted from the laser medium. The set of M starting pulses (corresponding to M longitudinal cavity modes) was assumed to have the probability density $W(I)=\exp(-I)$, for which the most probable, normalized, intensity of the N-th largest pulse has the value $\log(M/N)$. Clearly, the most important property of the fluctuation pattern is the ratio of the intensities of the two largest fluctuations at the end of the linear amplification stage. The probability that the largest pulse is more than R times as intense as the next largest can be shown to be, approximately, $R(M+1)^{R-1}$. If each pulse is assigned its most probable value, the ratio between the two largest pulses is ~1.18 and for $M=100$, the ratio will exceed this value for ~50% of the time.

Figure 2.40 illustrates the basic type of behaviour predicted by the fluctuation model of Glenn for the case of the modelocked Nd:glass laser, operating in a cavity of 5 ns round-trip time. The upper family of curves shows the development of the five largest pulses out of an ensemble of 100, when gain

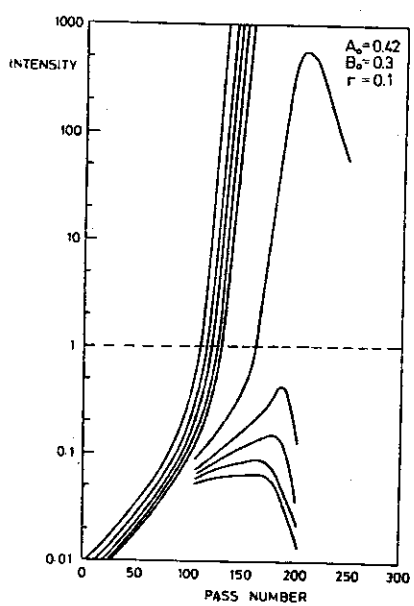

Fig. 2.40. Development of five largest pulses out of an ensemble of 100 for $B_0=0.3$, $\Gamma=0.1$ and $\Delta A=0.02$ at the start of the process. Upper curves show development when gain saturation is neglected and lower family of curves shows the effect of gain saturation (see text) (From Glenn [2.138]).

saturation is neglected and $B_0 = 0.3$, $\Gamma = 0.1$ and $\Delta A = 0.02$ at the start of the process. It is seen that discrimination is very weak and that the pulses grow without limit, which obviously cannot hold in practice. When saturable amplification is taken into account, the behaviour shown in the lower set of curves is predicted. The discrimination in favour of the most intense pulses is greatly increased by the slowing down of the rate of growth in the region of nonlinear amplification. As a result, a final intensity ratio of 2500 near the peak of the laser giant pulse is produced. The computations also showed that when B_0 is reduced to 0.2, the final ratio exceeds 9000, for an initial ratio of the intensity ratio of the two strongest pulses of only 1.02. This ratio would be exceeded 93% of the time.

These result clearly show that the most important parameter governing the behaviour of the laser is the excess gain $\Delta A = A - \Gamma - B_0$ existing at the start of the nonlinear phase of passive modelocking. For a small range of values of $\Delta A > 0$ the combination of the absorber nonlinearity and laser gain saturation provides sufficient discrimination to select the largest of the initial fluctuations, so as to produce a train of isolated single pulses. The important experimental result that the best mode locking of the Nd:glass laser is obtained by operating just above threshold ($\Delta A \leqslant 0.03$) is also obtained from the fluctuation model with gain saturation taken into account. When the excess gain is too low the intensity never breaks through the dye, but for higher gain discrimination is poor.

When the relaxation time T_{1b} of the absorber is longer than the mean duration of the fluctuation peaks at the end of the linear amplification stage, the fluctuation pulses of duration $< T_{1b}$ are poorly selected and can remain as noise spikes inside the final pulse intensity envelope. The optimum case occurs obviously [2.14] when $M \cong T/T_{1b}$ and then the most intense peak will be selected very effectively.

2.3.2 Passively Modelocked Dye Lasers

As we have seen in subsection 2.2.2, the generation of ultrashort pulses occurs very rapidly in modelocked dye lasers, and the final pulse durations are much shorter than the recovery times of the saturable absorbers employed. This very different behaviour of dye lasers, compared with solid state lasers, derives from the short (nanosecond) excited state lifetimes (T_{1a}) of the amplifying dye media. Because of the resulting short energy storage times, even flashlamp pumped dye lasers operate in a quasi-cw manner.

Employing a rate-equation analysis, *New* [2.102] first showed that in these circumstances amplifier and absorber saturation can combine to produce rapid pulse shortening, even when the pulse duration is already considerably shorter than both the gain and the absorber relaxation times. Later, the early stages of modelocking were analytically treated [2.139] and conditions were derived for the growth of oscillating perturbations. *Garside* and *Lim* [2.140, 141] employed a coherent field analysis and obtained similar numerical solutions

for both the buildup of the modelocking processes, and the eventual generation of ultrashort pulses. More recently *Haus* [2.120] has obtained a closed-form solution for the pulse intensity profile for the conditions under which cw modelocked dye lasers operate when a bandwidth-limiting element is used. Also *Yasa* et al. [2.142] have applied to dye lasers the computational model of *Gleun* [2.138] for the initial laser fluorescence fluctuation pattern to show numerically how these initial fluctuations evolve into a single picosecond pulses. *Yasa* and *Teschke* [2.143] have applied the same initial fluctuation pattern model to ultrashort pulse evolution in synchronously pumped dye lasers to obtain a stationary pulse solution. Reasonably good agreement with the experiments has been obtained with these various theoretical models, which are still being actively developed. It will be sufficient here to pick out the main points of the analyses and to show how they relate to the experimental results.

Rate-Equation Analysis

Frequency-dependent phenomena are explicitly left out in the rate-equation analysis, and as a result the ultimate pulse durations cannot be predicted quantitatively. However, the rate-equation approach is simple and provides particularly useful insight into pulse-compression mechanisms.

For pulses substantially shorter than either of the recovery times T_{1a} or T_{1b}, saturation is energy dependent and the pulse energy $j = \sigma_a \int_{-\infty}^{+\infty} F(\tau) d\tau$ [$F(\tau)$ is the photon flux at the local time $\tau = t - (x/c)$] obeys the energy balance equation [2.144]

$$A_L[1 - \exp(-j)] - B_L s^{-1}[1 - \exp(-sj)] - \Gamma j = 0 \qquad (2.28(a))$$

where A_L and B_L are the values of the respective coefficients at the leading edge of the pulse. The corresponding values in the trailing edge after the passage of a pulse are given by

$$A_T = A_L \exp(-j);\ B_T = B_L \exp(-sj). \qquad (2.28(b))$$

Γ is the linear loss and s is the important parameter introduced by *New* [2.103] the value of which is given by $s = kA_a\sigma_b/A_b\sigma_a$. A_a and A_b are the laser beam cross-sectional areas at the positions of the amplifier and absorber dyes, respectively. For an absorber dye cell in optical contact with a laser mirror, k has the value 2 [2.103] when the cell is thin compared with the pulse length.

New traced out the complete time development of a pulse, showing that the rate of pulse shortening is extremely rapid, and derived the regions of pulse compression in terms of the small signal laser gain, the round-trip time T, expressed in units of T_{1a}, and the value of s. The conclusions of the analysis were in good agreement with the experimental results, particularly that the best modelocking is achieved with high values of s and that the cavity length has to be adjusted to the correct value for optimum performance.

When the rate-equation analysis is applied to the early growth of modelocking in a ring dye laser the initial rate of buildup is found to be a strong function of the absorber relaxation times T_{1b}, being slow when T_{1b} is short, in agreement with the results obtained with cresyl-violet modelocked by DTDCI and DIC, described in *Temporal Buildup of Modelocking in Dye Lasers*. The minimum condition for modelocking

$$s(T_{1b}/T_{1a}) > A_u/B_u \tag{2.29}$$

is also obtained, where A_u and B_u are the unsaturated (small signal) amplification and absorption coefficients, respectively, per cavity transit.

Steady-State Pulse Solutions

Garside and *Lim* [2.140] applied standard density matrix formalism, with the rotating wave and the slowly varying envelope approximations, also to a ring dye laser to study modelocking conditions by a perturbation analysis. This analysis again showed that the recovery time of the absorber does not restrain the durations of the modelocked pulses. The results obtained by this approach were compared in detail [2.141] with those of *New* for both cw and flashlamp-pumped dye lasers. These authors further showed [2.141] that under typical experimental conditions flashlamp-pumped dye lasers can generate pulses that are close to being steady state. The wavelength dependence of the buildup of modelocking by DODCI in the rhodamine 6G dye laser (Fig. 2.24) also came out of the computations.

Haus [2.120] and *Haus* et al. [2.146] considered the situation when both the gain and loss per transit are relatively small ($\sim 20\%$). This situation is a good approximation to the cw dye laser case. These authors assumed that the saturable-absorber loss and the laser-medium gain coefficients could be expanded to second order in their pulse-energy dependence, and that the dispersion of the system, as a function of frequency, could be expanded to the second order in frequency (i.e., the laser pulse spectrum is narrow compared with either the laser dye fluorescence spectrum or the saturable-absorber bandwidth).

Closed-form analytic solutions were obtained to the steady-state equation

$$[I + l(t) - g(t) - (\Delta\omega)^{-2} d^2/dt^2] E(t) = -(\delta/\Delta\omega) dE(t)/dt \tag{2.30}$$

where $l(t)$, $g(t)$ are the loss and gain on transit through the absorbing and active media respectively; δ is a time delay (or advance) parameter proportional to any deviation δT of the pulse repetition period from the round-trip time T. The presence of a bandwidth-limiting element (tuning prism or etalon of bandwidth Δw) results in the introduction of the operator $-(\Delta\omega)^{-2} d^2/dt^2$, which leads to spreading of the pulse temporal profile. For the equilibrium

situation this pulse broadening is balanced by the pulse compression processes.

The conditions required to achieve modelocking with a saturable absorber of long relaxation time when expressed in terms of the same parameters, were similar to those of *New*, with quantitative discrepancies of only $\sim 10\%$. By approximating the excess-gain versus pulse energy curve by a parabola the steady-state pulse shape was shown to be a hyperbolic secant, with intensity $I(t)$ proportional to $\mathrm{sech}^2(t/\Delta t_p)$. The pulse width Δt_p was found to be inversely proportional to the disperser element bandwidth $\Delta\omega$, to the pulse energy, and to the square root of the small-signal value of the absorber loss $l(t)$. These predictions are in good agreement with the properties of the bandwidth-limited subpicosecond pulses obtained from the cw dye laser arrangement described in *Modelocked cw Dye Lasers*.

2.4 Picosecond Pulse Amplification

In Section 2.2 it was shown that, for a modelocked laser oscillator producing bandwidth-limited pulses, the energy content and peak powers of individual pulses were limited to the values 10^{-10} J (300 W) for the cw dye laser, 50 μJ (25 MW) from the flashlamp-pumped dye-laser and 1 mJ (200 MW) for giant-pulse solid-state lasers. For several applications of picosecond pulses amplifiers must be used to obtain greater energies, without producing either amplitude or frequency modulation of the oscillator pulses. The physical parameters affecting the design of picosecond pulse amplifiers, and limiting the performance, are the stimulated emission cross section σ, the lifetime of the upper laser level T_1, and the nonlinear refractive index n_2 of the host material.

Consider the rate equations, for a pulse travelling in the positive x direction through an amplifying medium [2.102, 147]

$$\dot{n} = (n_0 - n) T_1^{-1} - n\sigma F \tag{2.31}$$

and

$$\partial F/\partial x = n\sigma F \tag{2.32}$$

where F is the photon flux, n_0 is the population inversion at $F=0$, and the differentiation in (2.31) is with respect to the local time $\tau = t - (x/v)$, where v is the velocity of light in the medium. For picosecond pulses $T_1 \gg$ the pulse duration Δt_p and (2.31) gives

$$n(\tau) = n_i \exp(-\sigma J_\tau) \tag{2.33}$$

where

$$J_\tau = \int_{-\infty}^{\tau} F(\tau) d\tau. \tag{2.34}$$

n_i is the initial population inversion before the arrival of the pulse, and J_∞ represents the total pulse energy per unit area. Combining (2.32) and (2.33) yields

$$\partial F(\tau)/\partial x = n_i \sigma F \exp(-\sigma J_\tau). \tag{2.35}$$

Far out on the leading edge of a short pulse, travelling through an amplifier of length l, J_τ has a negligible value. The small signal gain for this portion of the pulse envelope is given by

$$g_{ss} = \exp(n_i \sigma l). \tag{2.36}$$

The total amplified energy density at the end of the amplifier is

$$E(l) = h\nu J_\infty(l) = h\nu\sigma^{-1} \ln\{1 + g_{ss}[\exp \sigma J_\infty(0) - 1]\}. \tag{2.37}$$

From (2.33), the saturation energy density (the energy density required to deplete the population inversion to e^{-1}) is

$$E_s = h\nu/\sigma. \tag{2.38}$$

When $E(0) \ll E_s$, the population inversion is not significantly changed by the passage of the pulse and the pulse profile is unaltered. When $E(0) \sim E_s$ amplification becomes nonlinear and the front of the pulse is more strongly amplified, whereas for $E(0) > E_s$ the stored energy is completely swept out by the pulse and the gain in energy depends only on the value of the total inversion. The size of the stimulated emission cross section affects amplifier design in other ways. If σ is too large, parasitic oscillations and amplified spontaneous emission (ASE) can, if suitable precautions are not taken, build up to a level where amplifier stored energy is seriously depleted. This problem arises particularly with dye laser systems where $\sigma \sim 10^{-16}$ cm^2. On the other hand, for efficient energy extraction at low pulse energies, a high value of σ is advantageous.

When an amplified picosecond pulse approaches a high enough power density, nonlinear refractive index effects begin to seriously affect the pulse properties. Whole beam self-focusing [2.148–150] occurs when the nonlinear phase shift builds up to 2π in a distance of $(2\pi/\lambda)\, a^2$, where a is the beam radius [2.151] and λ is the laser wavelength. The phase shift built up in a propagation distance l is given by

$$\Delta\phi \equiv B = (2\pi/\lambda)(\delta n/n_0) \int_0^l I(x)\,dx. \tag{2.39}$$

I is the light intensity, δn is the change in refractive index arising from the interaction of the laser beam and n_0 is the linear refractive index. For picosecond pulses the nonlinear refractive index can be regarded [2.152, 153] as

arising mostly from the nonlinear electronic polarizability (distortion of the electronic clouds). For glass the critical power for self-focusing of a uniform beam of gaussian cross section is $\sim 5 \times 10^6$ W. Small scale spatial fluctuations can cause self-focusing of portions of the beam at power levels well below those for total beam collapse [2.154, 155]. The most unstable spatial frequency grows according to the relation $I = I_0 \exp B$ [2.156]. The cumulative value of the B integral is thus a measure of the significance of nonlinear effects.

The intensity dependent index of refraction also produces self-phase modulation, as we have seen in the discussion of modelocked oscillators in Section 2.2. This frequency modulation is converted to modulation of the pulse temporal profile in the presence of linear dispersion [2.157]. Thus knowledge of the values of the nonlinear index n_2, and of the effects arising from n_2, is of great importance for the design of picosecond amplifiers.

2.4.1 Neodymium : Glass Amplifiers

The stimulated emission cross section for the host materials used in Nd:glass lasers are $\sim 3-5 \times 10^{-20}$ cm^2 [2.158]. The saturation energy density is ~ 5 J cm^{-2}, equivalent to a power density of 1 TW cm^{-2} for a pulse of 5 ps duration. However when the laser power density exceeds a few gigawatts per square centimetre nonlinear effects in the glass become apparent. Thus, any oscillator-amplifier system has to be operated under small-signal gain conditions, and the power density has to be maintained below the threshold levels for small-scale self-focusing and self-phase modulation. To reduce the possibility of small-scale self-focusing it is desirable to eliminate any small particles of dust or dirt on the optical surfaces and to reduce residual aberrations as much as possible. The most unstable spatial frequency corresponds to a structure of 100 μm dimension at a laser intensity of 10 GW cm^{-2} [2.156]. At the focus of a lens this structure falls outside the diffraction focus of the main beam. Thus, placing a limiting aperture (spatial filter) at the focus blocks the higher spatial frequencies and prevents the cumulative amplification of beam structures. The use of apodizing apertures [2.159] prevents the beam from developing diffraction fringes.

A picosecond Nd:glass laser system capable of amplifying a 5 ps pulse to an energy of 3 J (0.6 TW) is shown in Figure 2.41 [2.160]. This system employs a new phosphate glass LHG5 (Hoya) possessing a low value for n_2, zero refractive index temperature gradient (dn/dT) and a high stimulated emission cross section. The resulting increase in small-signal gain means that the amplifier pathlength can be shorter. Combined with the smaller value of n_2, this results in a reduced value of the B integral for a given overall amplification. Highly stable, TEM_{00} single-transverse mode, pulses of durations 3 to 10 ps and 1 mJ energy are obtained from the passively modelocked oscillator by switching out with a Kerr cell driven by a laser triggered spark gap. These pulses are passed through short length (15 to 20 cm) rod amplifiers to prevent self-focusing, self-phase modulation, amplified spontaneous emission and

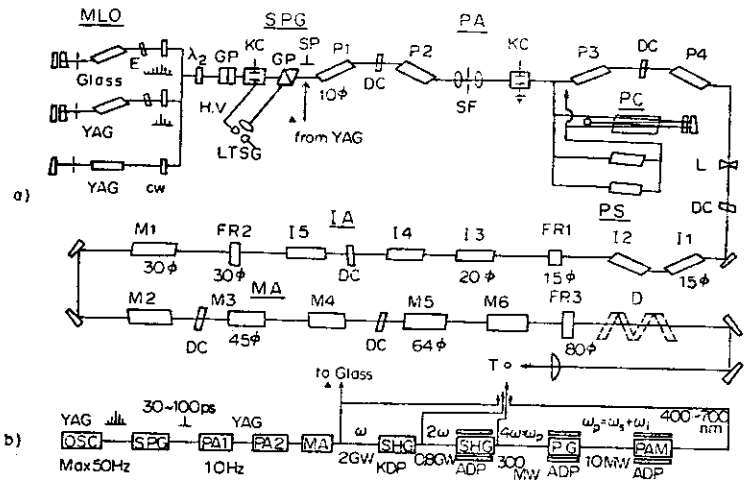

Fig. 2.41a and b. Experimental arrangement for (a) amplification and (b) frequency conversion of ultrashort pulses from Nd:glass and Nd:YAG lasers (from *Kuroda* et al. [2.160])

parasitic oscillation. The amplifiers are also decoupled and isolated by saturable absorber dye cells and by Faraday rotators with dielectric polarizers. The beam profile is cleaned up by spatial filtering. The final rod amplifier has a diameter of 64 mm and the power density is ~ 18 GW cm^{-2}.

New fluoride laser glasses with even smaller values of n_2 are under development [2.158] with gain coefficients and saturation parameters comparable to those of silicate glasses. These glasses should permit greater flexibility in the construction of picosecond amplifier systems.

Amplifier systems may also be used in conjunction with saturable absorbers to produce subpicosecond pulses [2.161, 162].

2.4.2 Amplification of Dye Laser Pulses

Dye laser amplifiers differ from Nd:glass systems in their disparate storage times of ~ 5 ns and ~ 300 μs, respectively. As a result, in a flashlamp-pumped dye laser amplifier it is only the energy stored during the 5 ns or so before the arrival of a picosecond pulse that contributes. Because of the large stimulated emission cross section ($\sigma \sim 10^{-16}$ cm^2) dye amplifier dimensions are limited by the need to avoid ASE losses, which are significant even with low stored energy densities. Also, as already discussed, the large cross section results in a high small-signal gain and a low saturation energy density (~ 3 mJ cm^{-2}).

Amplification to peak powers of >3 GW have been achieved with the arrangement shown in Fig. 2.42 [2.33]. Modelocking of an aqueous solution of rhodamine 6G (Rh6G) by an ethanolic solution of DODCI covered the spectral range 595 to 625 nm while the region 575 to 600 nm was covered by modelocking an ethanolic solution of Rh6G by DQOCI. The pulses employed for amplification studies had durations of ~ 2 ps, as measured with a streak camera, and the corresponding spectral bandwidths (FWHM) were ~ 2 nm. The first amplifier employed a 5 mm internal diameter dye cell, and the second amplifier a 1 cm diameter dye cell. Firing of the two amplifiers was synchronized to ± 100 ns and maximum gain always occurred at the peak of the 5 μs flashlamp pulse. With the system aligned and firing only the amplifiers, up to 500 mJ of ASE was emitted from the second amplifier. This arose, in part, from reflection from the oscillator output mirror and could be overcome by employing ethanolic solutions of Rh6G. Then ASE occurred mainly at wavelengths shorter than 585 nm. When amplifying pulses of wavelengths >600 nm a solution of 3,3'-dimethylthiacyanine iodide placed between the oscillator and the first amplifier selectively absorbed the ASE.

Alternatively, when the ASE was not spectrally different from the picosecond pulses, a Fabry-Perot filter was used as isolator. Small signal gain measurements were carried out, for each amplifier independently, by attenuating the oscillator output one-hundred fold. Fig. 2.43 gives the variation of peak small-signal amplifier gain with wavelength, for different dye solutions and shows the importance of choosing the correct amplifying solution for optimising small-signal gain at a particular wavelength. To obtain the wavelength dependence of gain in the saturated regime (σ varies with wavelength (Fig. 2.43) and hence the value of the saturation energy density E_s) the unattenuated oscillator beam was passed through the first amplifier and the beam area telescoped down to 3 mm^2 before the second amplifier. From Fig. 2.44 it can be seen that, with the energy densities employed, the gain at each wavelength diminishes rapidly from its small-signal value to a wavelength in-

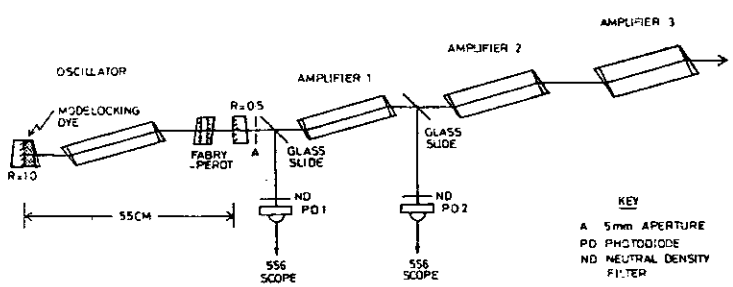

Fig. 2.42. Schematic diagram of modelocked dye-laser oscillator and amplifier chain for amplification of picosecond pulses to powers of >3 GW (from *Adrain* et al. [2.33])

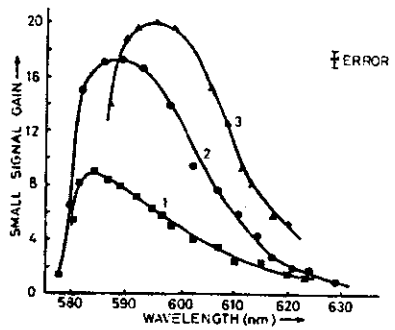

Fig. 2.43. Variation of small signal gain with wavelength for. (1) 10 mm diameter amplifier (9×10^{-5} M Rh 6G in ethanol), (2) 5 mm diameter amplifier (1.5×10^{-4} M Rh 6G + 10^{-5} M Rh B in ethanol), (3) 5 mm diameter amplifier (2.5×10^{-4} M Rh 6G in water)

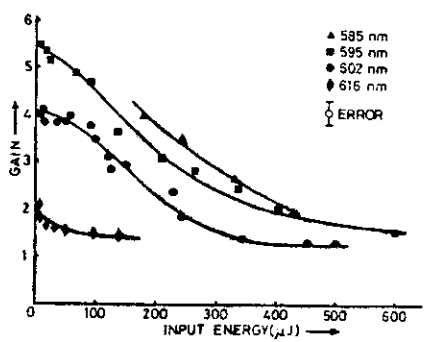

Fig. 2.44. Gain of 10 mm diameter dye laser amplifier at four wavelength as a function of input picosecond pulse energy

dependent saturated gain of ~1.4. These results clearly show how the amplification of picosecond pulses in a dye laser amplifier varies with both wavelength and input pulse energy density. As an example, a 70 μJ pulse, at 605 nm, can be amplified to ~1 mJ in the first amplifier and to ~4 mJ in the second amplifier. A third amplifier of 15 mm internal diameter pumped by 4 ablative lamps further increases the pulse energy to ~7 mJ, corresponding to a peak power of 3.5 GW. Streak-camera measurements of the amplified pulses showed no shortening of the pulse durations. Any self-steepening effect [2.157] would be masked by nonlinear self-action.

At these power densities self-phase modulation produced spectral broadening of the pulses by ~0.1 nm in the first (water solution) amplifier and by ~0.4 nm in the second (ethanolic solution) amplifier. Knowing the laser power density, the values $n_2 = 1.4 \times 10^{-13}$ esu for water and $n_2 = 4.5 \times 10^{-13}$ for ethanol can be calculated [2.150], in good relative agreement with the measured ratio of 4:1 for the values of n_2 for ethanol and water [2.163].

A nitrogen laser pumped amplifier is a better match to the storage time of a laser dye, since the pumping pulses last only a few nanoseconds. It is also possible to arrange the relative timing of the N_2 laser pulse so that one selected pulse of the modelocked train is amplified. Single-pulse selector electro-optical switches are then not required. *Schmidt* [2.164] has used this approach to amplify ~2.5 μJ pulses, from a modelocked flashlamp-pumped rhodamine 6G laser, in a cell containing a rhodamine B solution transversely pumped by the beam from an N_2 laser (3 mJ in 8 ns). The entrance and exit windows of the amplifier cell were anti-reflection coated and tilted to avoid feedback. The pumped region had dimensions 10 mm by 0.1 mm by 0.1 mm, and the oscillator beam was telescoped down to an area of 0.25 mm^2 to give an input energy density of ~1 mJ cm^{-2}. The amplified pulse of ~100 μJ was thus well above the saturation energy density. Further stages of amplification or a more powerful N_2 pumping laser should provide greater pulse energies. Since the nitrogen laser is an effective pump for a large number of dyes this method could be employed for the amplification of synchronously modelocked dye lasers, with their wider spectral coverage.

An alternative approach to amplification of the pulses from a modelocked oscillator is the modelocking of high-power laser oscillators by injection locking to a low-power modelocked signal from a cw laser, as proposed by *Moses* et al. [2.165]. This method has the advantage of locking the spectral and directional properties of the high-powered pulsed laser to those of the cw beam. Gains of $\sim 3 \times 10^4$ have been demonstrated [2.165] with a cw Rh6G dye laser, modelocked by synchronous pumping with a modelocked argon-ion laser operating at 5145 Å. The flashlamp-pumped Rh6G laser shared a common mirror (reflectivity 96%) with the cw laser. The optical lengths of the three lasers were precisely matched, employing a second-harmonic autocorrelation interferometer. When all the cavity lengths were matched (without the flashlamp being fired) the amplitude of the second-harmonic signal increased suddenly accompanied by a corresponding increase in the width of the cw lasing spectrum. The flashlamp-pumped system was spectrally controlled by a birefringent electro-optical tuner [2.166]. A birefringent Lyot filter in the cw laser gave a ~0.2 nm bandwidth, and tuning over the entire range of the dye for both lasers was obtained without realignment. The bandwidth of the flashlamp-pumped system was ~0.1 nm and good pulses were obtained near threshold. The pulse durations lengthened from 15 ps (of the cw laser) to 20 ps, corresponding to a time-bandwidth product, $\Delta\nu\Delta t$, value of ~2. Provided that bandwidth-limited pulse durations were maintained, this technique could be useful for the amplification of ~300 W peak power subpicosecond pulses

from the passively modelocked cw dye laser [2.118, 167]. Also several high-power flashlamp-pumped lasers could be modelocked, synchronised and aligned by a single cw oscillator [2.168].

2.5 Frequency Changing

Harmonic generation provides the easiest means of producing picosecond pulses at short wavelengths. Apart from satisfying the normal phase-matching conditions (see *Akhmanov* et al. [2.169] for an excellent review of optical harmonic generation and optical frequency multipliers) group velocity mismatch has to be taken into account. For efficient harmonic generation it is necessary to have the optical path length L in the nonlinear material shorter than the group velocity characteristic length $L_{gl} = \Delta t / \Delta u^{-1}$ where $\Delta u^{-1} (\equiv u_N^{-1} - u_1^{-1})$ is the group velocity mismatch parameter and u_1, u_N are the group velocities of the fundamental and N-th harmonic frequencies, respectively. The group velocity mismatch for the commonly used nonlinear crystals is given in Table 2.4. It can be seen that the effect is large in $LiNbO_3$ and $LiIO_3$ for 1.06 μm pulses and is even larger for ultraviolet frrquency multipliers. When $L < L_{gl}$ (the quasi-static regime), if the fundamental pulse has a gaussian intensity temporal profile, the harmonic pulse is also gaussian with the duration reduced by a factor $\sqrt{N}$ and the bandwidth increased by the same factor. When $L > L_{gl}$ the width of the harmonic spectrum narrows [2.170] and the pulse duration increases during propagation through the crystal to the value $L.\ \Delta u^{-1}$. This effect has been demonstrated for second-harmonic generation of Nd:glass laser picosecond pulses in KDP and in $LiNbO_3$ [2.171]. The spectral width and the harmonic pulse duration also depend strongly on the beam divergence [2.172]. On the positive side, the threshold intensities for optical breakdown in crystals increase for ultrashort pulses as the inverse of the laser pulse duration [2.173] and reach values of 10^{10} to 10^{11} W cm^{-2} for picosecond pulses.

Akhmanov et al. [2.174] generated the fourth-harmonic frequency of picosecond pulses from a Nd:glass laser by successive second-harmonic generation in KDP crystals, with an overall energy conversion efficiency of 2%. The laser was operating in many transverse modes and self-phase modulation probably

Table 2.4. Characteristic group-delay length L_{gl} for second-harmonic generation of a 1 ps pulse

Fundamental wavelength	L_{gl} cm			
	KDP	$LiNbO_3$	$LiIO_3$	CDA
1.06 μm	3.7	0.2	0.5	1.4
0.53 μm	0.3	—	—	—

(From Akhmanov et al. [2.169])

was affecting the temporal profiles of the pulses. Phase modulation can result in a deviation from the optimal phase-matching relationship when there is group velocity mismatch. Energy is then pumped back into the fundamental frequency [2.175]. With breakup of the temporal profile due to self-action effects, group velocity mismatch will certainly come into play. *Kung* et al. [2.176] obtained 80% efficiency for frequency doubling, and 10% efficiency for cascade tripling of bandwith-limited 50 ps pulses from a Nd:YAG laser. Employing an intracavity cesium dihydrogen arsenate (CDA), 90° phase-matched, second-harmonic generator *Weisman* and *Rice* [2.73] generated trains of pulses of nearly equal energies at the fundamental and harmonic frequencies of a Nd:glass laser. The second-harmonic bandwidth was narrowest when phase matching was optimized by temperature tuning the CDA crystal and operation of the modelocked laser was then at its most stable (pulse duration ~9 ps). This indicated that self-focusing and self-phase modulation were being suppressed by the nonlinear loss introduced by the harmonic generator [2.177].

Second-harmonic generation of pulses from synchronously pumped cw dye lasers over the uv spectral region from 265 nm to 335 nm has been obtained using RhB, Rh6G and Na-fluorescein dyes. The pulse duration of the Rh6G laser was 7.5 ps at 600 nm and was bandwidth limited. With angle-tuned KDP crystals the energy conversion efficiency was ~0.05% giving uv average powers of 50 to 250 μW. With 90° phase-matched ADP a conversion efficiency of 2% was measured at 270 nm. The authors of this publication expect to achieve an average (modelocked) uv output power of 5 mW from Rh6G with a 90° phase-matched ADA harmonic generator. *Ippen* and *Shank* [2.178] reported conversion to the uv of the pulses from a passively modelocked dye laser by frequency doubling in a $LiIO_3$ crystal, of thickness 0.25 mm. The large nonlinear coefficient of this material more than compensates for the shorter characteristic group-delay length. Visible pulses with a peak power of ~5 kW can be converted to produce ~1 ps, 307.5 nm pulses with ~15% efficiency.

Pulses from dye lasers synchronously pumped by a modelocked Nd:YAG laser had been sum and difference mixed with both the fundamental and the second-harmonic pulses of the pumping laser, to generate tunable ultrashort pulses in the uv from 270 to 432 nm, and in the ir from 1.13 to 5.6 μm. This technique has the advantages over optical parametric generators [2.179, 180] in that large beam divergences and broad spectral bandwidths are avoided. Also lower input power levels are required since the mixing process does not start from parametric noise. The modelocked Nd:YAG oscillator trains of 30 ps pulses (in a TEM_{00} beam of ~3 mJ total energy and a transform-limited bandwidth of ~0.1 nm) were amplified (sevenfold energy gain) and frequency doubled in a KDP crystal (energy conversion 30%). The dye laser was frequency narrowed and tuned by two Fabry-Perot etalons, of 6 μm and 100 μm spacings, to produce 12 ps bandwidth-limited pulses in a linearly polarized TEM_{00} mode from Rh6G. With RhB, cresyl-violet perchlorate, and carabizine 122 dyes a continuous tuning range of 549 to 727 nm was covered. Sum-

mixing of the dye laser pulses with 1.064 m pulses in KDP generated pulses from 362 to 432 nm with an efficiency of 20% at 369 nm, the efficiency being primarily proportional to the 1.064 μm power. Sum-mixing the dye laser pulses with the 532 nm pulse train in ADP covered the spectral range from 270 to 307 nm. Difference mixing with 1.064 m radiation in $LiIO_3$ produced ir pulses tunable from 1.1 to 2.3 μm with ~2% efficiency and with 532 nm pulses the range 1.98 to 5.6 μm was covered. In all cases phase matching by angle tuning the crystals at room temperature was employed.

Nonlinear crystals capable of phase-matched harmonic generation are not transparent at wavelengths shorter than ~200 nm. Thus to reach the vacuum ultraviolet (vuv) gases and metal vapours must be employed as the nonlinear media for phase-matched harmonic generation. Third-order nonlinear processes in isotropic media [2.181] have been employed for the production of tunable [2.182] and fixed frequency [2.183] vuv radiation. Employing 30 ps pulses (peak powers $\sim 3 \times 10^8$ W) from a modelocked Nd:YAG laser, *Bloom* et al. [2.184] generated the third-harmonic frequency in a phase-matched mixture of rubidium and xenon with 10% energy conversion efficiency. Using the same laser system *Bloom* et al. [2.185] obtained frequency tripling in a homogeneous mixture of sodium and magnesium vapour with ~4% energy efficiency. Tripling in Rb-Xe mixtures has also been achieved with 7 ps pulses from a Nd:glass laser (2×10^8 W) with 2% energy conversion [2.186]. A further stage of frequency tripling to 118.2 nm radiation had been obtained earlier [2.187, 188]. Starting with a single pulse (25 ps, 3×10^8 W) at 1.064 μm frequency doubled in ADP to 532 nm and mixed, also in ADP, to give 354.7 nm radiation (peak power 10^7 W), the uv pulse was then frequency tripled in a phase-matched mixture of Xe and Ar to produce a vuv pulse at 118.2 nm. (Later, more careful measurements of the conversion efficiency of this stage revealed that the original measurement of 2.8% efficiency was too high by a factor of 20 [2.188].)

Employing a modelocked dye laser [2.189] it was possible to tune close to a two-photon resonance in calcium so as to enhance the nonlinear susceptibility [2.190] for third-harmonic generation. Pulses from a flashlamp-pumped Rh6G laser (2 ps, 50 μJ) were amplified to peak powers of ~300 MW and focused into calcium vapour, phase matched by xenon. The durations of the 200 nm pulses, measured by a streak camera, were the same those of the fundamental frequency pulses (~4 ps). With two simultaneously driven dye lasers, synchronously pumped and modelocked by a common Nd:glass laser, *Royt* et al. [2.191] generated frequency-tunable 9 ps pulses in the vuv (190 to 195 nm) by four-wave mixing in strontium vapour. Resonant enhancement for both the two-photon and the single-photon frequencies was achieved. The conversion efficiency was 10^{-5} for power densities of 5×10^8 W cm^{-2} at the two-photon transition wavelength and was 5×10^7 W cm^{-2} at the second dye-laser wavelength.

Picosecond pulses at 173.6 nm for amplification by the Xe_2 vuv laser have been obtained with the arrangement of Fig. 2.45 [2.192, 193] by mixing fundamental frequency (50 MW) and second-harmonic pulses from a modelocked ruby laser in magnesium vapour phase matched by xenon. There is a near two-photon resonance in magnesium for one ruby second-harmonic photon plus one fundamental-frequency photon (Fig. 2.46). A peak power of 200 W at 173.4 nm corresponded to a power conversion efficiency of 4×10^{-6}. Amplification of the oscillator pulses could provide vuv megawatt, picosecond pulses if saturation or optical Stark shifts do not affect the conversion efficiency [2.194]. Further frequency tripling in argon to the xuv (at 57.8 nm) could then be produced, after amplification if necessary by an excimer Xe_2 laser. This step has recently been achieved [2.195] for the megawatt, nanosecond pulses

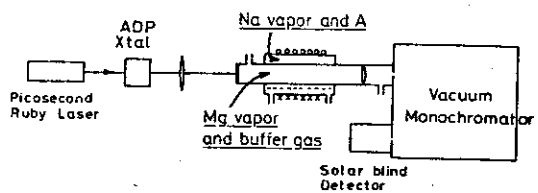

Fig. 2.45. Experimental arrangement for the generation of the fourth-harmonic frequency of a modelocked ruby laser. After the second-harmonic generation in ADP, one second-harmonic photon is sum-mixed with two fundamental photons in magnesium vapour phase matched by xenon (from *Bradley* [2.192])

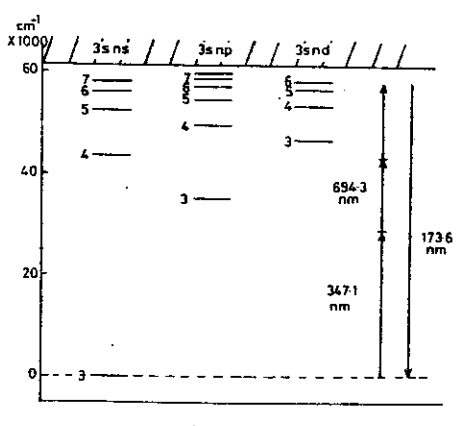

Fig. 2.46. Energy level diagram of Mgl showing the transients involved in two-photon resonance-enhanced four-wave mixing

from a frequency tunable Xe_2 laser [2.193, 195]. In this way xuv picosecond pulses could be obtained at useful powers.

In this chapter we have reviewed the methods of generating picosecond pulses by modelocked lasers. In the xuv region coherent generation has just recently been obtained [2.195], and new techniques are also being developed for the ir region. For example, ultrashort pulses can also be generated by an optical analogue of NMR free induction decay (FID) [2.197, 198]. Subnanosecond 10.6 μm pulses have been produced by sharply terminating a long duration CO_2 pulse by optical breakdown, and then passing it through a narrow CO_2 absorber [2.199]. Nearly total absorption occurred until the absorber reradiated a short FID pulse upon input pulse termination. Direct pulse observation as well as autocorrelation techniques [2.200, 201] have inferred pulses as short as 30 to 50 ps.

References

2.1 H.W. Mocker, R.J. Collins: Appl. Phys. Lett. **7**, 270 (1965)
2.2 A.J. DeMaria, C.M. Ferrar, G.E. Danielson: Appl. Phys. Lett. **8**, 22 (1966)
2.3 A.E. Siegman, D.J. Kuizenga: Opto. Electronics, **6**, 43 (1974)
2.4 P.W. Smith: Proc. IEEE **58**, 1342 (1970)
2.5 J. de Vries, D. Bebelaar, J. Langelaar: Opt. Commun. **18**, 24 (1976)
2.6 E.D. Jones, M.A. Palmer, F.R. Franklin: Opt. Quant. Elect. **8**, 231 (1976)
2.7 A.J. Alcock, A.C. Walker: Appl. Phys. Lett. **25**, 299 (1974)
2.8 E.R. Pike (Ed.): *High Power Gas Lasers*, 1975, Proceedings of Summer School on Physics and Technology of High-Power Gas Lasers, Capri, 1975, Conference Series No. 29, (Institute of Physics, Bristol and London 1975)
2.9 H. Kogelnik, T. Li: Appl. Opt. **5**, 1550 (1966); Proc. IEEE **54**, 1312 (1966)
2.10 P.W. Smith: Proc. IEEE **60**, 422 (1972)
2.11 M. Born, E. Wolf: *Principles of Optics*, 3rd Edition (Pergamon Press, New York 1965) p. 494
2.12 L. Mandel, E. Wolf: Rev. Mod. Phys. **37**, 231 (1965)
2.13 D.J. Bradley, G.H.C. New: Proc. IEEE **62**, 313 (1974)
2.14 P.G. Kryukov, V.S. Letokhov: IEEE J. QE-**8**, 766 (1972)
2.15 E.K. Zavoiskii, S.D. Fanchenko: Sov. Phys. Doklady **1**, 285 (1956)
2.16 T. Ohmi, S. Hasuo, S. Hari: J. Appl. Phys. **43**, 3773 (1972)
2.17 J.A. Giordmaine, P.M. Rentzepis, S.L. Shapiro, K.W. Wecht: Appl. Phys. Lett. **11**, 218 (1967)
2.18 A.J. DeMaria, W.H. Glenn, M.J. Brienza, M.E. Mack: Proc. IEE **57**, 2 (1969)
2.19 H.P. Weber: Phys. Lett. **27A**, 321 (1968)
2.20 J.R. Klauder, M.A. Duguay, J.A. Giordmaine, S.L. Shapiro: Appl. Phys. Lett. **13**, 174 (1968)
2.21 D.J. Bradley, G.H.C. New, S.J. Caughey: Phys. Lett **30A**, 78 (1969)
2.22 D.J. Bradley, T. Morrow, M.S. Petty: Opt. Commun. **2**, 1 (1970)
2.23 D.J. Bradley, M.H.R. Hutchinson, H. Koetser, T. Morrow, G.H.C. New, M.S. Petty: Proc. Roy. Soc. (London) **328A**, 97 (1972)
2.24 N. Ahmad, B.C. Gale, M.H. Key: Advan. Electron. Phys. **28B**, 999 (1969)
2.25 D.J. Bradley, J.F. Higgins, M.H. Key: Appl. Phys. Lett. **16**, 53 (1970)
2.26 D.J. Bradley: UK Patent Spec. 31167/70 (1970); U.S. Patent 3761614 (1973)
2.27 D.J. Bradley, B. Liddy, W.E. Sleat: Opt. Commun. **2**, 391 (1971)
2.28 M. Ya. Schelev, M.C. Richardson, A.J. Alcock: Appl. Phys. Lett. **18**, 354 (1971)

2.29 P.R. Bird, D.J. Bradley, W. Sibett: Proc. 11th Intern. Congr. High Speed Photography, ed. by P.J. Rolls (Chapman and Hall, London 1974) p. 112
2.30 D.J. Bradley, W. Sibbett: Appl. Phys. Lett. **27**, 382 (1975)
2.31 D.J. Bradley: Opto-Electronics **6**, 25 (1974)
2.32 E.G. Arthurs, D.J. Bradley, B. Liddy, F. O'Neill, A.G. Rodd, W. Sibbett, W.E. Sleat: Proc. 10th Intern. Congr. High Speed Photography (A.N.R.T. Paris 1972) p. 117
2.33 R.S. Adrain, E.G. Arthurs, D.J. Bradley, A.G. Roddie, J.R. Taylor: Opt. Commun. **12**, 136 (1974)
2.34 R.S. Adrain, E.G. Arthus, W. Sibbett: Opt. Commun. **15**, 290 (1975)
2.35 D.J. Bradley, A.G. Roddie, W. Sibbett, M.H. Key, M.J. Lamb, C.L.S. Lewis, P. Sachsenmaier: Opt. Commun. **15**, 231 (1975)
2.36 N.G. Basov, M.M. Butslov, P.G. Kriukov, Yu.A. Matveets, E.A. Smirnova, S.D. Fanchenko, S.V. Chekalin, R.V. Chikin: Preprint 82, Lebedev Phys. Inst. Moscow, USSR (1972)
2.37 S.D. Fanchenko, B.A. Frolov: Sov. Phys. JETP Lett. **16**, 101 (1972)
2.38 M.M. Butslov, A.A. Malyutin, A.M. Prokhorov, B.M. Stepanov, M. Ya. Schelev: Proc. 10th Intern. Congr. High-Speed Photography (A.N.R.T. Paris 1972) p. 122
2.39 M. Ya. Schelev: Proc. 11th Congr. High-Speed Photography, ed. by P.J. Rolls (Chapman and Hall, London 1974) p. 32
2.40 J. Nuckolls, L. Wood, A. Thiessen, G. Zimmerman: Nature **239**, 139 (1972)
2.41 S.E. Harris, J.F. Young, A.H. Kung, D.M. Bloom, G.C. Bjorklund: In *Laser Spectroscopy*, ed. by R.G. Brewer, A. Mooradian (Plenum Press, New York and London 1974) p. 59
2.42 D.J. Bradley: In *Lecture notes in Physics*, Vol. 43: *Laser Spectroscopy* (Springer, Berlin, Heidelberg, New York 1975) p. 55
2.43 D.J. Bradley, M.H.R. Hutchinson, C.C. Ling: In *Springer Series in Optical Sciences*, Vol. 3: Tunable Lasers and Applications, Proceedings of the Leon Conference, Norway 1976, ed. by A. Mooradian, T. Jaeger, P. Stokseth (Springer, Berlin, Heidelberg, New York 1976) p. 40
2.44 B.L. Henke, J.A. Smith, D.T. Attwood: 1976 (unpublished)
2.45 P.R. Bird, D.J. Bradley, A.G. Roddie, W. Sibbett, M.H. Key, M.J. Lamb, C.L.S. Lewis: Proc. 11th Congr. High Speed Photography, ed. by P.J. Rolls (Chapman and Hall, London 1974) p. 118
2.46 G.I. Bryukhnevitch, Yu.S. Kasyanov, V.V. Korobkin, A.M. Prokhorov, B.M. Stepanov, V.K. Chevokin, M. Ya. Schelev: Proc. 11th Intern. Congr. High Speed Photography, ed. by P.J. Rolls (Chapman and Hall, London 1974) p. 554
2.47 Yu.S. Kasyanov, A.A. Malyutin, M.C. Richardson, V.K. Chevokin: Proc. 11th Intern. Congr. High Speed Photography, ed. by P.J. Rolls (Chapman and Hall, London 1974) p. 561
2.48 C.F. McConaghy, L.W. Coleman: Appl. Phys. Lett. **25**, 268 (1974)
2.49 A.J. Lieber, H.D. Sulphin, C.B. Webb: Abstract of paper at Intern. Conf. Physics of x-ray spectra, Gaithersburg, August 1976 (unpublished)
2.50 D.J. Bradley: 1976 (unpublished)
2.51 S.W. Thomas, J.W. Houghton, G. Tripp, L.W. Coleman: Proc. 11th Intern. Congr. High Speed Photography, ed. by P.J. Rolls (Chapman and Hall, London 1974) p. 101
2.52 G. Jeah-Francois, P. Nodenot, V.V. Korobkin, Yu.V. Korobkin, A.V. Prokhindeev, M. Ya. Schelev: Proc. 11th Intern. Congr. High Speed Photography, ed. by P.J. Rolls (Chapman and Hall, London 1974) p. 190
2.53 G. Porter: Opt. Commun. **18**, 141 (1976); private communication (1975)
2.54 L.A. Lompre, G. Mainfray, J. Thebault: Appl. Phys. Lett. **26**, 500 (1975)
2.55 R. Hadland, K. Helbrough, A.E. Huston: Proc. 11th Intern. Congr. High Speed Photography, ed. by P.J. Rolls (Chapman and Hall, London 1974) p. 107; K. Helbrough, M.C. Adams, W. Sibbett, T.H. Williams: Abstract of paper read at 12th Intern. Congr. High Speed Photography, Toronto, August 1976
2.56 D.J. Bradley: Proc. 11th Intern. Congr. High Speed Photography, ed. by P.J. Rolls (Chapman and Hall, London 1974) p. 23
2.57 D.J. Bradley, M.H.R. Hutchinson, H. Koetser: Proc. Roy. Soc. London **A329**, 105 (1972)

2.58 D.J. Bradley, W. Sibbett: Opt. Commun. 9, 17 (1973)
2.59 N.G. Basov, M.M. Butslov, P.G. Krykov, Yu.A. Matveets, E.A. Smirnova, B.M. Stepanov, S.D. Franchenko, S.V. Chekalin, R.V. Chikin: Soviet Phys. JETP 38, 449 (1974)
2.60 D. von der Linde: IEEE J. QE-8, 328 (1972)
2.61 M.A. Duguay, J.W. Hansen, S.L. Shapiro: IEEE J. QE-6, 725 (1970)
2.62 D.J. Bradley, G.H.C. New, S.J. Caughey: Opt. Commun. 2, 41 (1970)
2.63 E.M. Gordeev, P.G. Kryukov, Yu.A. Matveets, B.M. Stepanov, S.D. Fanchenko, S.V. Chekalin, A.V. Sharkov: Sov. J. Quantum. Electron. 5, 129 (1975)
2.64 M.C. Richardson: IEEE J. QE-9, 768 (1973)
2.65 F. DeMartini, C.H. Townes, T.K. Gustafson, P.L. Kelley: Phys. Rev. 164, 312 (1967)
2.66 R.A. Fisher, P.L. Kelley, T.K. Gustafson: Appl. Phys. Lett. 14, 140 (1969)
2.67 V.V. Korobkin, A.A. Malyutin, M.Ya. Schelev: Sov. Phys. JETP Lett. 11, 103 (1970)
2.68 R.C. Eckardt, C.H. Lee, J.N. Barford: Opto-Electronics 6, 67 (1974)
2.69 D.J. Bradley, G.H.C. New, S. Caughey: Phys. Lett. 33A, 313 (1970)
2.70 N.E. Bykovskii, V. Kan, P.G. Kryukov, Yu.A. Matveets, N.L. Ni, Yu.V. Senatskii, S.V. Chekalin: Sov. J. Quant. Electron. 2, 56 (1972)
2.71 S.V. Chekalin, P.G. Mryukov, Yu.A. Matveets, O.B. Shatkerashvilii: Opto-Electronics 6, 249 (1974)
2.72 M.H.R. Hutchinson: PhD Thesis, The Queen's University of Belfast (1971)
2.73 R.B. Weisman, S.A. Rice: Spectros. Lett. 8, 329 (1975)
2.74 N.G. Basov, Yu.A. Drozhbin, P.G. Kryukov, V.B. Lebedev, V.S. Letokhov, Yu.A. Matveets: Sov. Phys. JETP Lett. 9, 256 (1969)
2.75 N. Nakashima, N. Mataga: Chem. Phys. Lett. 35, 487 (1975)
2.76 E.D. Jones, M.A. Palmer: Opt. Quant. Electron. 7, 520 (1975)
2.77 A.N. Zherikhin, V.A. Kovalenko, P.G. Kryukov, Yu.A. Matveets, S.V. Chekalin, O.B. Shatberashivili: Sov. J. Quant. Electron. 4, 210 (1974)
2.78 A.W. Penney, H.A. Heynau: Appl. Phys. Lett. 9, 257 (1966)
2.79 W.R. Hook, R.H. Dishington, R.P. Hilberg: Appl. Phys. Lett. 9, 125 (1966)
2.80 G. Kachen, L. Steinmetz, J. Kysilka: Appl. Phys. Lett. 13, 229 (1968)
2.81 M. Michon, H. Guillet, D. Le Goff, S. Raynaud: Rev. Sci. Instr. 40, 263 (1969)
2.82 A.J. Alcock, M.C. Richardson: Opt. Commun. 2, 65 (1970)
2.83 D. von der Linde, O. Bernecker, A. Laubereau: Opt. Commun. 2, 215 (1970)
2.84 R.C. Hyer, H.D. Sutphin, K.R. Winn: Rev. Sci. Instr. 46, 1333 (1975)
2.85 D.J. Bradley, A.J.F. Durrant: Phys. Lett. 27A, 73 (1968)
2.86 D.J. Bradley, A.J.F. Durrant, G.M. Gale, M. Moore, P.D. Smith, IEEE J. QE-4, 707 (1968)
2.87 W.H. Glenn, M.J. Brienza, A.J. DeMaria: Appl. Phys. Lett. 12, 54 (1968)
2.88 B.H. Soffer, J.W. Linn: J. Appl. Phys. 39, 5859 (1968)
2.89 D.J. Bradley, A.J.F. Durrant, F. O'Neill, B. Sutherland: Phys. Lett. 30A, 535 (1969)
2.90 W. Schmidt, F.P. Schafer: Phys. Lett. 26A, 558 (1968)
2.91 D.J. Bradley, F. O'Neill: Opto-Electronics 1, 69 (1969)
2.92 E.G. Arthurs, D.J. Bradley, A.G. Roddie: Appl. Phys. Lett. 19, 480 (1971)
2.93 E.G. Arthurs, D.J. Bradley, A.G. Roddie: Appl. Phys. Lett. 20, 125 (1972)
2.94 D.J. Bradley, B. Liddy, A.G. Roddie, W. Sibbett, W.E. Sleat: Opt. Commun. 3, 426 (1971)
2.95 D.J. Bradley, B. Liddy, W. Sibbett, W.E. Sleat: Appl. Phys. Lett. 20, 219 (1972)
2.96 E.G. Arthurs, D.J. Bradley, A.G. Roddie: Appl. Phys. Lett. 23, 88 (1973)
2.97 E.G. Arthurs, D.J. Bradley, A.G. Roddie: Chem. Phys. Lett. 22, 230 (1973); Opt. Commun. 8, 118 (1973)
2.98 E.G. Arthurs, D.J. Bradley, P.N. Puntambekar, I.S. Ruddock, T.J. Glynn: Opt. Commun. 12, 360 (1974)
2.99 E.G. Arthurs, D.J. Bradley, T.J. Glynn: Opt. Commun. 12, 136 (1974)
2.100 D.N. Dempster, T. Morrow, R. Rankin, G.F. Thompson: J. Chem. Soc. Faraday II 68, 1479 (1972)
2.101 D. Madge, M.W. Windsor: Chem. Phys. Lett. 27, 31 (1974)
2.102 G.H.C. New: Opt. Commun. 6, 188 (1972)

2.103 G.H.C. New: IEEE J. QE-10, 115 (1974)
2.104 A.G. Roddie: PhD Thesis, The Queen's University of Belfast (1072)
2.105 R.S. Adrain: PhD Thesis, The Queen's University of Belfast (1974)
2.106 F.P. Schafer, W. Schmidt, W. Marth: Phys. Lett. 24A, 280 (1967)
2.107 G. Mourou, G. Busca, M.M. Denariez-Roberge: Opt. Commun. 4, 40 (1971)
2.108 D.J. Bradley, T. Morrow, M.S. Petty: Opt. Commun. 2, 1 (1970); M.S. Petty: PhD Thesis, The Queen's University of Belfast (1970)
2.109 J.C. Mialocq, A.W. Boyd, J. Jaraudias, J. Salton: Chem. Phys. Lett. 37, 236 (1976)
2.110 G.E. Busch, R.P. Jones, P.M. Rentzepis: Chem. Phys. Lett. 18, 178 (1973)
2.111 G. Mourou, B. Drouin, M.M. Denariez-Roberge: Appl. Phys. Lett. 20, 453 (1972)
2.112 H.E. Lessing, E. Lippert, W. Rapp: Chem. Phys. Lett. 7, 227 (1970)
2.113 D. Kuizenga: Appl. Phys. Lett. 19, 260 (1971)
2.114 A. Dienes, E.P. Ippen, C.V. Shank: Appl. Phys. Lett. 19, 258 (1971)
2.115 E.P. Ippen, C.V. Shank, D. Dienes: Appl. Phys. Lett. 21, 348 (1972)
2.116 F. O'Neill: Opt. Commun. 6, 360 (1972)
2.117 E.P. Ippen, C.V. Shank: Appl. Phys. Lett. 27, 488 (1975)
2.118 I.S. Ruddock, D.J. Bradley: Appl. Phys. Lett. 29, 296 (1976)
2.119 C.V. Shank, E.P. Ippen: Appl. Phys. Lett. 24, 373 (1974)
2.120 H.A. Haus: IEEE J. QE-11, 736 (1975); Opt. Commun. 15, 29 (1975)
2.121 T.R. Royt, W.L. Faust, L.S. Goldberg, C.H. Lee: Appl. Phys. Lett. 25, 514 (1974)
2.122 L.S. Goldberg, C.A. Moore: Appl. Phys. Lett. 27, 217 (1975); & Opt. Commun. 16, 21 (1976).
2.123 L.S. Goldberg, C.A. Moore: Lecture Notes in Physics, Vol. 43: *Laser Spectroscopy* (Springer, Berlin, Heidelberg, New York 1975) p. 248; Opt. Commun. 16, 21 (1976).
2.124 C.K. Chan, S.O. Sari: Appl. Phys. Lett. 25, 403 (1974)
2.125 C.K. Chan, S.O. Sari, R.E. Foster: J. Appl. Phys. 47, 1139 (1976)
2.126 H. Mahr, M.D. Hirsch: Opt. Commun. 13, 96 (1975)
2.127 J.M. Harris, R.M. Chrisman, F.E. Lytle: Appl. Phys. Lett. 26, 16 (1975)
2.128 H. Mahr: private communication (1976)
2.129 P.K. Runge: Opt. Commun. 4, 195 (1971)
2.130 P.K. Runge: Opt. Commun. 5, 311 (1972)
2.131 Z.A. Yasa, O. Teschke: Appl. Phys. Lett. 27, 446 (1975)
2.132 B. Fan, T.K. Gustafson: Appl. Phys. Lett. 28, 202 (1976)
2.133 D. Roess: J. Appl. Phys. 37, 2004 (1966)
2.134 V.S. Letokhov: Soviet Phys. JETP 28, 562 (1969); Sov. Phys. JETP, 28, 1026 (1969)
2.135 J.A. Fleck: Appl. Phys. Lett. 12, 178 (1968); J. Appl. Phys. 39, 3318 (1968)
2.136 J.A. Fleck: Phys. Rev. B. 1, 84 (1970)
2.137 W.H. Glenn: ~~IEEE~~ Rep. No. L920935-8, United Aircraft Corp. (1972)
2.138 W.H. Glenn: IEEE J. QE-11, 8 (1975)
2.139 G.H.C. New, D.H. Rea: J. Appl. Phys. ~~(in press 1976)~~ 47, 3107 (1976).
2.140 B.K. Garside, T.K. Lim: J. Appl. Phys. 44, 2335 (1973); Opt. Commun. 12, 8 (1974)
2.141 B.K. Garside, T.K. Lim: Opt. Commun. 12, 240 (1974)
2.142 Z.A. Yasa, O. Teschke, L.W. Bravermans, A. Dienes: Opt. Commun. 15, 354 (1975)
2.143 Z.A. Yasa, O. Teschke: Opt. Commun. 15, 169 (1975)
2.144 G.H.C. New, K.E. Orkney, M.J.W. Nock: Optical and Quant. Electron. ~~(in press 1976)~~ 8, 425 (1976)
2.145 P.G. Kryukov, V.S. Letokhov: Sov. Phys. Usp. 12, 641 (1971)
2.146 H.A. Haus, C.V. Shank, E.P. Ippen: Opt. Commun. 15, 29 (1975)
2.147 A. Icsevgi, W.E. Lamb: Phys. Rev. 185, 517 (1969)
2.148 R.Y. Chiao, E. Garmire, C.H. Townes: Phys. Rev. Lett. 13, 479 (1964)
2.149 P.L. Kelley: Phys. Rev. Lett. 15, 1005 (1965)
2.150 S.A. Akhmanov, R.V. Khoklov, A.P. Sukhorukov: In *Laser Handbook*, ed. by F.T. Arecchi, E.O. Schultz-Dubois (North Holland Publ. Co., Amsterdam 1972) p. 1151
2.151 E.L. Dawes, J.H. Marburger: Phys. Rev. 179, 862 (1969)
2.152 R.C. Brewer, C.H. Lee: Phys. Rev. Lett. 21, 267 (1968)
2.153 R.R. Alfano, S.L. Shapiro: Phys. Rev. Lett. 24, 592 (1970); 24, 1217 (1970)
2.154 A.J. Campillo, S.L. Shapiro, B.R. Suydam: Appl. Phys. Lett. 23, 628 (1973); 24, 178 (1974)

2.155 E. S. Bliss, D. R. Speck, J. F. Holzrichter, J. H. Erkkila, A. J. Glass: Appl. Phys. Lett. **25**, 448 (1974)
2.156 J. Trenholme: Lawrence Livermore Lab. Rep., U.C.R.L. 50021-74 (1975) p. 178
2.157 R. A. Fisher, W. K. Bischel: J. Appl. Phys. **46**, 4921 (1975)
2.158 M. J. Weber, C. B. Layne, R. A. Saroyan, D. Milam: Opt. Commun. **18**, 171 (1976)
2.159 P. Jacquinot, B. Roizen-Dossier: In *Progress in Optics*, ed. by E. Wolf (North Holland Publ. Co., Amsterdam 1964) Vol. III, p. 130
2.160 H. Kuroda, H. Masuko, S. Maekawa: Opt. Commun. **18**, 169 (1976)
2.161 A. Penzkofer, D. von der Linde, A. Laubereau, W. Kaiser: Appl. Phys. Lett. **20**, 351 (1972)
2.162 A. Penzkofer: Opto-Electronics, **6**, 87 (1974)
2.163 W. Wernicke, A. Law, M. Pfeiffer, K. Lenz, H. J. Weigmann, C. D. Thuy: Opt. Commun. **4**, 413 (1972)
2.164 A. J. Schmidt: Opt. Commun. **14**, 287 (1975)
2.165 E. I. Moses, J. J. Turner, C. L. Tang: Appl. Phys. Lett. **28**, 258 (1976); Opt. Commun. **18**, 24 (1976); Appl. Phys. Lett. **27**, 441 (1975)
2.166 J. M. Telle, C. L. Tang: Appl. Phys. Lett. **24**, 85 (1974); **26**, 572 (1975)
2.167 I. S. Ruddock, W. Sibbett, D. J. Bradley: Opt. Commun. **18**, 26 (1976)
2.168 T. S. Ruddock: PhD Thesis, University of London (1976)
2.169 S. A. Akhmanov, A. I. Kovrygin, A. P. Sukhorukov: In *Nonlinear Optics*, ed. by H. Rabin, C. C. Tang (Academic Press, New York, London 1975) p. 475 and references therein
2.170 S. A. Akhmanov, A. P. S. Sukhorukov, A. S. Chirkin: Sov. Phys. JETP **55**, 1480 (1968)
2.171 S. L. Shapiro: Appl. Phys. Lett. **13**, 19 (1968)
2.172 R. Yu. Orlov, A. S. Chirkin, T. Usmanov: Sov. Phys. JETP **57**, 1069 (1969)
2.173 D. F. Fradin, N. Bloembergen, J. Letellier: Appl. Phys. Lett. **22**, 635 (1973)
2.174 S. A. Akhmanov, I. B. Skidan, R. Yu. Orlov, L. I. Telegrin: Sov. Phys. JETP Lett. **16**, 471 (1972)
2.175 Yu. N. Karamzin, A. P. Sukhorukov: Sov. J. Quant. Electron. **5**, 496 (1975)
2.176 A. Kung, J. F. Young, G. Bjorklund, S. E. Harris: Phys. Rev. Lett. **29**, 985 (1972)
2.177 J. E. Murray, S. E. Harris: J. Appl. Phys. **41**, 609 (1970)
2.178 E. P. Ippen, C. V. Shank: Opt. Commun. **18**, 27 (1976)
2.179 R. L. Byer: In *Nonlinear Optics*, ed. by H. Rabin, C. L. Tang (Academic Press, New York, London 1975) p. 587 and references therein
2.180 S. E. Harris: Proc. IEEE **57**, 2096 (1969)
2.181 J. F. Ward, G. H. C. New: Phys. Rev. **185**, 57 (1969)
2.182 R. T. Hodgson, P. P. Sorokin, J. J. Wynne: Phys. Rev. Lett. **32**, 343 (1974)
2.183 S. E. Harris, J. F. Young, A. H. Kung, D. M. Bloom, G. C. Bjorklund: In *Laser Spectroscopy*, ed. by R. G. Brewer, A. Mooradian (Plenum Press, New York and London 1974) p. 59
2.184 D. M. Bloom, G. W. Bekkers, J. F. Young, S. E. Harris: Appl. Phys. Lett. **26**, 687 (1975)
2.185 D. M. Bloom, J. F. Young, S. E. Harris: Appl. Phys. Lett. **27**, 390 (1975)
2.186 H. Puell, C. R. Vidall: Opt. Commun. **18**, 107 (1976)
2.187 A. H. Kung, J. F. Young, S. E. Harris: Appl. Phys. Lett. **22**, 301 (1973)
2.188 A. H. Kung, J. F. Young, S. E. Harris, Erratum: Appl. Phys. Lett. **28**, 239 (1975)
2.189 W. Sibbett, D. J. Bradley, S. F. Bryant: Opt. Commun. **18**, 107 (1976)
2.190 P. D. Maker, R. W. Terhune, C. M. Savage: Proc. III Int. Conf. Quantum Electron, Paris 1964, p. 1559
2.191 T. R. Royt, C. H. Lee, W. L. Faust: Opt. Commun. **18**, 108 (1976)
2.192 D. J. Bradley: In *Laser Spectroscopy*, ed. by S. Haroche, J. C. Pebay-Peyroula, T. W. Hansch, S. E. Harris (Springer, Berlin, Heidelberg, New York 1975) p. 55
2.193 E. G. Arthurs, D. J. Bradley, C. B. Edwards, S. Domanski, D. R. Hull, C. C. Ling, M. H. R. Hutchinson: In *Proc. Intern. Conf. Electron Beam Research and Technology*, ed. by G. Yonas (Sandia Laboratories, SAND 76-5122, 1976) p. 193
2.194 J. N. Elgin, G. H. C. New: Opt. Commun. **16**, 242 (1976)
2.195 M. H. R. Hutchinson, C. C. Ling, D. J. Bradley: Opt. Commun. ~~(in press)~~ **18**, 203 (1976)
2.196 D. J. Bradley, D. R. Hull, M. H. R. Hutchinson, M. W. McGeoch: Opt. Commun. **7**, 187 (1975)

2.197 S. L. McCall: PhD Thesis, Univ. of Calif., Berkeley (1968)
2.198 D. C. Burnham, R. Y. Chiao: Phys. Rev. **188**, 667 (1969)
2.199 E. Yablonovitch, J. Goldhar: Appl. Phys. Lett. **25**, 580 (1974)
2.200 B. J. Feldman, R. A. Fisher, E. J. McLellan, S. J. Thomas: Opt. Commun. **18**, 72 (1976)
2.201 E. Yablonovitch, H. S. Kwok: Opt. Commun. **19**, 103 (1976)